Electric field control of magnetism using BiFeO3-based heterostructures

J. T. Heron, D. G. Schlom, and R. Ramesh

Citation: Applied Physics Reviews **1**, 021303 (2014); doi: 10.1063/1.4870957
View online: http://dx.doi.org/10.1063/1.4870957
View Table of Contents: http://scitation.aip.org/content/aip/journal/apr2/1/2?ver=pdfcov
Published by the AIP Publishing

APPLIED PHYSICS REVIEWS

Electric field control of magnetism using $BiFeO_3$-based heterostructures

J. T. Heron,[1,a)] D. G. Schlom,[1,2] and R. Ramesh[3,4,5,6]
[1]*Department of Materials Science and Engineering, Cornell University, Ithaca, New York 14853, USA*
[2]*Kavli Institute at Cornell for Nanoscale Science, Ithaca, New York 14853, USA*
[3]*Department of Materials Science and Engineering, University of California, Berkeley, California 94720, USA*
[4]*Department of Physics, University of California, Berkeley, California 94720, USA*
[5]*Materials Science Division, Lawrence Berkeley National Laboratory, Berkeley, California 94720, USA*
[6]*Oak Ridge National Laboratory, Oak Ridge, Tennessee 37831, USA*

(Received 9 February 2014; accepted 13 March 2014; published online 22 April 2014)

Conventional CMOS based logic and magnetic based data storage devices require the shuttling of electrons for data processing and storage. As these devices are scaled to increasingly smaller dimensions in the pursuit of speed and storage density, significant energy dissipation in the form of heat has become a center stage issue for the microelectronics industry. By taking advantage of the strong correlations between ferroic orders in multiferroics, specifically the coupling between ferroelectric and magnetic orders (magnetoelectricity), new device functionalities with ultra-low energy consumption can be envisioned. In this article, we review the advances and highlight challenges toward this goal with a particular focus on the room temperature magnetoelectric multiferroic, $BiFeO_3$, exchange coupled to a ferromagnet. We summarize our understanding of the nature of exchange coupling and the mechanisms of the voltage control of ferromagnetism observed in these heterostructures. © *2014 AIP Publishing LLC*. [http://dx.doi.org/10.1063/1.4870957]

TABLE OF CONTENTS

[a)]Author to whom correspondence should be addressed. Electronic mail: jth247@cornell.edu

I. INTRODUCTION

CMOS technology is seeing growing barriers to scaling and increased energy efficiency as the demand for higher density and lower power consumption devices becomes imperative, and thus the search for new technologies to augment or replace CMOS have increased.[1] Spintronics, a field of research that seeks to employ the electron spin in devices in addition to its charge,[2,3] has emerged with devices poised to improve information processing[4–7] and information storage.[8–10] Many of these new technologies rely on the spin transfer torque (STT), where the injection of a spin-polarized current is used to drive the motion of a magnetic domain wall or change the magnetic state of a magnetic multilayer device.[11,12] While STT memories provide the historical advantages of magnetic based memories (such as high speed, high density, and high reliability all in a non-volatile technology), it does not sufficiently lower energy dissipation. A large current density of $\sim 10^5$–10^6 A/cm^2 is typically required for STT switching making resistive losses the primary source of power

consumption.[13,14] As an example of the energy consumption of such a device, a state of the art STT device requires a voltage pulse of several hundred millivolts (0.7 V) and 120 ps[14]–500 ps[13] in duration through a 60–70 nm × 180 nm device leading to energy dissipation per unit area per switch of 3–4 mJ/cm^2. The effort to reduce this energy cost has led to the pursuit of mechanisms by which magnetic anisotropy and magnetization direction can be tailored with an applied electric field, rather than electrical current, where, in an ideal case, the energy dissipation per unit area can be estimated to be at least an order of magnitude smaller.

A revival of interest in materials or heterostructures that possess more than one ferroic parameter has been driven by the interest in studying the correlations between two or more ferroic orders[15] and the possibility of demonstrating next generation devices using these correlations. Materials of this class are deemed multiferroic.[16,17] Originally, the definition of multiferroics was limited to single-phase materials that simultaneously display one of the four ferroic orders: ferroelectricity, ferromagnetism, ferroelasticity, and ferrotoroidicity.[18] This definition has been broadened to include materials that possess antiferroic order, such as antiferromagnetism, as well. The incorporation of multiferroics in devices should not only enable additional functionality through the multiple controllable order parameters but also through the coupling of the multiple order parameters.[19,20] Magnetoelectricity or magnetoelectric coupling (the coupling of the ferroelectric and magnetic orders), which can enable the electric field control of magnetism, observed in both single-phase and composite multiferroics have been under intense investigation and summarized in many review articles.[16,17,21–25] Due to the many reviews on the topic, this review is not written to give the reader a detailed review of multiferroics and all of the pathways to the electric field control of magnetism[26,27] enabled by this materials class. Rather, we focus on the room temperature single-phase magnetoelectric multiferroic $BiFeO_3$ (BFO) and its integration into exchange coupled heterostructures where it serves as an electrically controllable pinning layer. The appeal of such a configuration is that it combines the intrinsic magnetoelectric coupling, which couples the ferroelectric order to the magnetic order of $BiFeO_3$, and the interface exchange coupling with the ferromagnetic layer, thereby coupling the moments of the ferromagnet to the magnetic order of $BiFeO_3$, giving rise to a pathway of controlling a large ferromagnetic magnetization with solely an applied electric field. As noted previously, electric field control of magnetism is attractive to the spintronics community in that the significant energy dissipation arising from Joule heating can be eliminated. Since the writing/switching of the large magnetization in these $BiFeO_3$/ferromagnet heterostructure is governed by the ferroelectric switching of the multiferroic, the energy consumption of an ideal device can easily be estimated if parasitic losses (such as leakage) are ignored. Taking the saturation polarization (along [001] ~ 60 μC/cm^2) and the switching voltage (1–5 V) of an (001) oriented $BiFeO_3$ film that is nominally 100–200 nm thick, the estimated energy dissipation per unit area per switch is 120–600 μJ/cm^2, about an order of magnitude smaller than the consumption of a optimized STT device. The remainder of this review focuses on summarizing the observations of exchange coupling and the magnetoelectric switching of $BiFeO_3$/ferromagnet heterostructures. Furthermore, in the case of thin films, this review highlights the challenges and directions toward the advancement of this materials system in applications of low-energy consumption devices.

A. $BiFeO_3$: A room temperature single-phase magnetoelectric multiferroic

$BiFeO_3$ has been the most heavily investigated single-phase multiferroic to date largely due to the coexistence of its magnetic order and ferroelectric order at ambient conditions. Interestingly, the research of $BiFeO_3$ dates to well before the discovery of its thin film stabilization in 2003.[28,29] Much, as it is now, of early investigations of $BiFeO_3$ focused on its magnetoelectric coupling; however, these studies investigated bulk crystals rather than thin films, which dominate $BiFeO_3$ research now.[30] At an early stage, $BiFeO_3$ was determined to crystallize in the $R3c$ perovskite structure (i.e., a rhombohedrally distorted perovskite)[31,32] and display a ferroelectric hysteresis[33] and a G-type antiferromagnetic spin lattice that cants to forms a long-range spin cycloid that propagates along the {110} directions.[34,35] As has now been confirmed in the bulk, the electric polarization of the epitaxially stabilized thin film is ~90 μC/cm^2. Disparate from the bulk, however, is the breaking of the spin cycloid in thin films, instead favoring a long-range weak canted magnetization that preserves the G-type antiferromagnetic order.[36]

Figs. 1(a)–1(c) show the rhombohedrally distorted perovskite crystal structure, a G-type antiferromagnetic lattice, and the canting of the $BiFeO_3$ antiferromagnetic spins in the (111) plane forming the weak magnetization. Since the rhombohedral distortion is small, crystal orientations in the literature (and in this paper) frequently refer to a cubic unit cell. Fig. 1(a) shows the $BiFeO_3$ crystal structure in the two different bases. The main instability that drives the formation of the ferroelectric polarization is the ordering of Bi lone pairs where the outer Bi 6s electrons are highly polarizable and orient along the direction of the rhombohedral distortion (the [111] direction) below ~1100 K.[33,37,38] The G-type antiferromagnetic order is driven by the super-exchange interaction between neighboring d^5 – Fe^{3+} atoms and mediated by the O^{-2} between them. The half-full d-shell of the Fe^{3+} atoms and the occupied O^{-2} p orbitals promotes the configuration where all nearest neighbor spins point (arrows represent Fe^{3+} spins) antiparallel to one another as in Fig. 1(b) making the spins in the (111) plane ferromagnetically aligned. The antiferromagnetic ordering temperature (Néel temperature) was measured to be 643 K,[39] significantly lower than the ferroelectric ordering temperature. This difference has significant ramifications on the strength of the magnetoelectric interaction since the magnetoelectric coupling must result as the consequence of a weaker interaction, which is in this case the spin-orbit driven Dzyaloshinskii-Moriya (DM) interaction.[40–42] These latter two points, naturally, have profound implications on the symmetries that govern the magnetoelectric switching in $BiFeO_3$.[36,43,44] Furthermore, the symmetry of the rhombohedrally distorted perovskite and the

rotation of the oxygen octahedral cages permit the formation of a weak magnetic moment through a canting of the antiferromagnetic lattice via the torque provided by the DM interaction: $E = -\frac{1}{2}\vec{D} \cdot (\vec{M}_1 \times \vec{M}_2)$. Here, $\vec{D}$ is the DM vector, which is highly dependent on symmetry. The DM interaction can be rewritten in a form specific to $BiFeO_3$ to highlight the mutual orthogonality of its macroscopic orders and the expected magnetoelectric switching permissible[36]

$$E \sim \vec{P} \cdot (\vec{L} \times \vec{M}_c). \quad (1)$$

The ferroelectric polarization can point along any one of the eight degenerate $\langle 111 \rangle$ directions. This degeneracy, along with a consideration of the electrostatic and elastic boundary conditions, permits the possible formation of three "flavors" (i.e., 71°, 109°, and 180°) of domain walls that are distinguished by the angle the polarization rotates across the domain wall (see Figs. 1(d) and 1(e)).[45] Typically, piezoresponse force microscopy (PFM), a scanning probe technique that employs a conductive tip to apply a localized electric field, is used to determine the flavor of the domain wall by mapping the direction of the polarization in each of the domains. The piezoelectric coefficient of a ferroelectric is dependent on its polarization direction, thus the out-of-plane component of the polarization can be inferred from the phase offset of the PFM tip with respect to the phase of the applied ac voltage and the in-plane (IP) component can be inferred from the shear forces experienced by the tip.[46] IP and out-of-plane PFM images of two $BiFeO_3$ films deposited by pulsed laser deposition on $SrTiO_3$ (STO) substrates at different deposition rates (controlled by the frequency of the laser pulses) are shown in Figs. 2(a) and 2(b) with the film in (b) having the faster rate. A thorough review of the synthesis of $BiFeO_3$ (and many other oxides) thin films can be found in Ref. 47. The deposition rate influences domain formation and the primary flavor of domain wall to populate the film.[48] Figs. 2(c) and 2(d) trace out the domain walls present in the two films. The domain structure in Fig. 2(a), a so called 4-variant film due to the presence of only 4 of the 8 possible polarization directions, is primarily composed of 71° domain walls while the domain structure in Fig. 2(b), referred to as a mosaic or disordered domain structure, is predominantly 109° domain walls.

As is the case with $BiFeO_3$, multiferroics that support both ferroelectric and magnetic orders are typically insulators with an antiferromagnetic spin arrangement (and possibly a very small magnetization from spin canting). Hence, to achieve electric field control of conductive ferromagnets with large magnetization for device applications, multiferroics are studied in ferromagnet-multiferroic exchange coupled heterostructures. Section II is dedicated to the exchange coupling of transition metal and oxide ferromagnets to $BiFeO_3$ to highlight the different mechanisms of exchange anisotropy in these structures.

II. EXCHANGE COUPLING IN FERROMAGNET/$BiFeO_3$ HETEROSTRUCTURES

Despite its relevance to the electric field control of magnetism in an exchange coupled heterostructure, it is surprising that the details of exchange coupling have not received more attention in reviews of the electric field control of magnetism. It is the goal of this section to summarize our knowledge in exchange coupled ferromagnet/$BiFeO_3$ heterostructures and highlight the experimental knobs that can be tuned to engineer the magnetic properties of the system. We also discuss potential issues that may pose as challenges to future endeavors but leave a detailed discussion for Sec. IV. Finally, we hope that this section promotes exchange coupling as an investigative tool for uncovering magnetic order in multiferroics.

The broad interest in ferromagnetic-antiferromagnetic heterostructures originates from the initial discovery of exchange bias observed by Meiklejohn-Bean in 1956

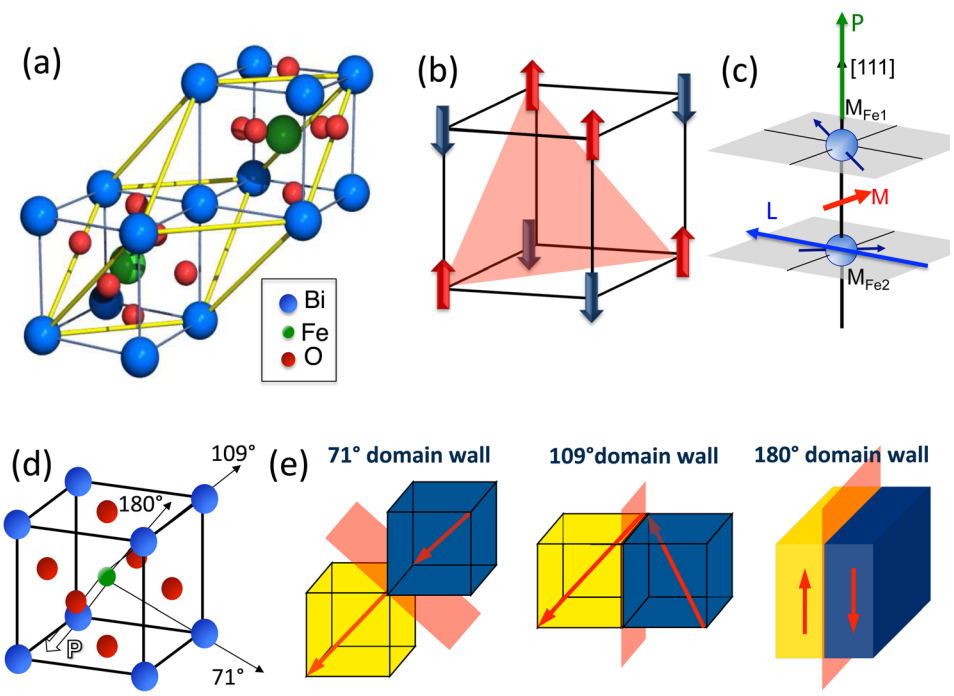

FIG. 1. (a) Rhombohedral (yellow) and cubic (blue) unit cells of $BiFeO_3$. (b) Schematic of a G-type antiferromagnet highlighting the ferromagnetic order within the (111) plane. (c) Schematically illustrating that the antiferromagnetic spins in $BiFeO_3$ lie in the (111) plane and the canting of these spins produces a small magnetization (M) which lies in this plane. (d) Schematic of the cubic unit cell of $BiFeO_3$ with a polarization (P—white arrow) along one of the $\langle 111 \rangle$ directions. Black arrows indicate the permissible angles of rotation the polarization can make either due to an applied electric field or across a domain wall. (e) Schematics of the three "flavors" of domain walls permitted in $BiFeO_3$.

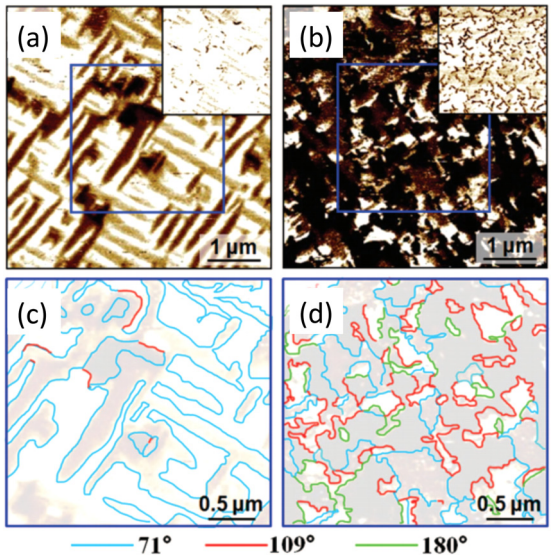

FIG. 2. (a) and (b) IP PFM (and out-of-plane PFM: insets) images of two $BiFeO_3$ films deposited on $SrTiO_3$ substrates at different deposition rates. (c) and (d) Line traces of the domain walls present in the two films highlighting that the domain structure and the composition of the domain walls can be tuned with deposition rate. The domain structure in (a) is primarily 71° domain walls while that in (b) is largely 109° domain walls. Reprinted with permission from Martin *et al*., Nano Lett. **8**, 2050 (2008). Copyright 2008 American Chemical Society.

(Ref. 49) and its pervasive use in the magnetic read heads found in hard drives.[50,51] Exchange bias manifests as a shift (either positive or negative) in the ferromagnetic hysteresis loop of the ferromagnetic-antiferromagnetic heterostructure, breaking the symmetry about zero magnetic field.[52–57] Typically to observe such an effect, the antiferromagnetic layer must be cooled in a magnetic field below the Néel temperature to align the antiferromagnetic spins, however, when the Néel temperature is high, exchange bias is present when the soft ferromagnetic layer is deposited on the antiferromagnet while under a small magnetic field. In the phenomenological description of exchange bias by Meiklejohn and Bean (a simple Stoner-Wohlfarth model[58,59]), the spins at the surface of the antiferromagnetic layer are ferromagnetically ordered and ferromagnetically coupled to the surface spins in the ferromagnetic layer. While this picture is quite simple, the origin of the exchange bias effect is still understood to be an interface effect driven by pinned uncompensated spins at the surface of the antiferromagnet. Difficulties typically arise in the quantification of the effect and understanding the source of the uncompensated spins. On compensated surfaces, the uncompensated spins are attributed to extrinsic defects in the antiferromagnet such as surface roughness,[60–62] vacancies,[63] and domain walls.[64] Exchange bias is not the only manifestation of exchange coupling observable in a magnetic hysteresis loop; the coercive field of the exchange coupled heterostructure will broaden with respect to the coercive field of the uncoupled ferromagnetic layer. The broadening of the hysteresis is attributed to the dragging of unpinned spins in the antiferromagnet due to the rotation of the spins in the ferromagnetic layer in response to an applied magnetic field. In this case the interface coupling energy is larger than the product of the volume anisotropy energy of the antiferromagnet and its thickness. In many ferromagnet-antiferromagnet heterostructures both coercivity broadening and exchange bias will be present indicating that both pinned and unpinned spins in the antiferromagnet are present at the interface. For excellent reviews on exchange coupling and quasi-static modeling see Refs. 52–57, and 65.

A. Exchange coupling with transition metal ferromagnets (TMFs)

The strong correlations in $BiFeO_3$ are exemplified by its ferroelectric, ferroelastic, and (anti)ferromagnetic orders and the coupling between them. In such correlated materials, it is expected that at domain boundaries, where there are changes in the electric, magnetic, and elastic states, intriguing behavior, disparate from the bulk, should appear.[66,67] In $BiFeO_3$ bulk crystals, the antiferromagnetic structure is cycloidal G-type with a period of $\lambda_{\langle 110\rangle} = 64$ nm (Refs. 34, 35, and 69), while in thin films a weak ferromagnetic moment emerges from the breaking of this cycloid.[36] Thus, the nature and strength of the exchange coupling is expected to vary from bulk crystal to thin film and with the domain wall density and flavor (i.e., 71°, 109°, 180°).

1. Single domain bulk crystals

While the exchange coupling between $BiFeO_3$ multidomain films and monodomain single crystals is significant, the anisotropies of the two systems are remarkably different.[48,68–70] Additionally, thin film heterostructures have the benefit that the magnetic anisotropy of the system can be engineered with epitaxy.[71–74] In monodomain single crystals, the exchange coupled TMF acquires a uniaxial anisotropy along the propagation vector of the antiferromagnetic spin cycloid of $BiFeO_3$ (see Fig. 3).[68,69] A broadening of the hysteresis is observed while exchange bias is absent indicating that an insignificant density of pinned uncompensated spins lies on the (001) surface of the $BiFeO_3$ crystal. The Heizenberg exchange energy is minimized when the cycloid moments and the TMF moments are parallel and the demagnetization energy is minimized when the TMF are stacked tip-to-tail. The competition between these two energy states favors a TMF magnetization that "wiggles" in-phase with the oscillation of the spin cycloid and the TMF moments stack nearly tip-to-tail in the direction of the cycloid propagation direction.[69]

2. Multidomain thin films: Effect of domain walls

In thin film based heterostructures, the magnetic anisotropy is dependent on the domain structure, domain wall density, and the flavor of the domain walls. The works of Refs. 48 and 70 have combined PFM and magnetometry measurements to show that a unidirectional anisotropy (exchange bias) scales with the inverse of the ferroelectric domain size of $BiFeO_3$. In $BiFeO_3$, the ferroelectric and antiferromagnetic domains are coupled so that the antiferromagnet domain size and structure can be inferred from PFM measurements.[75] By mapping the length and flavor of domain walls present for both a 4-variant (primarily 71°

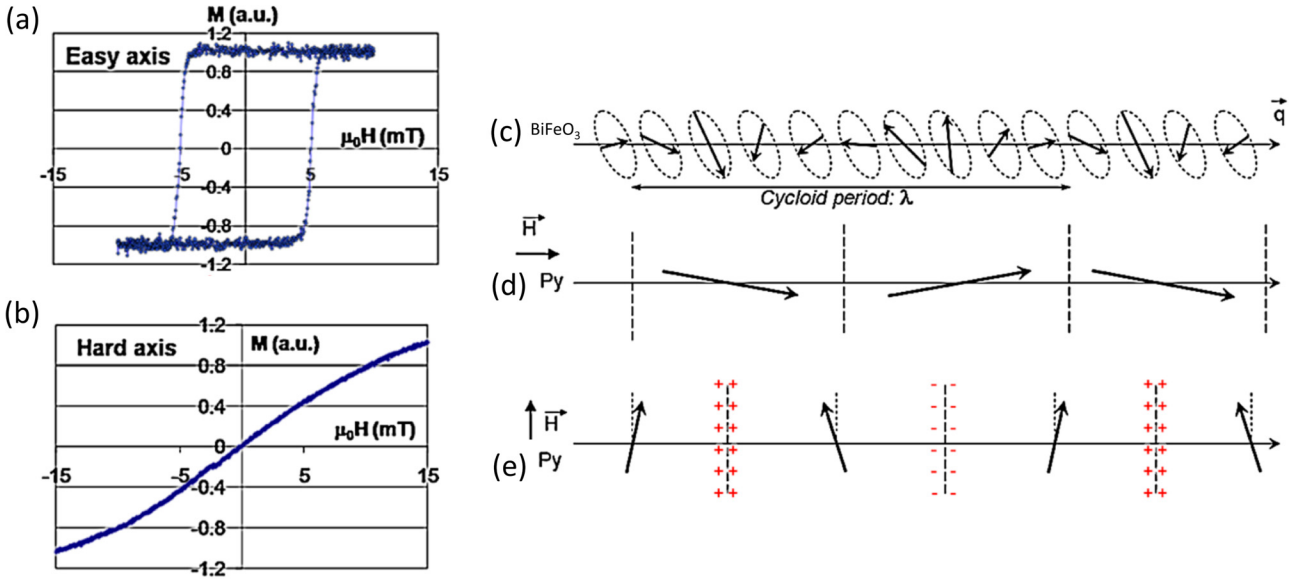

FIG. 3. Depiction of the exchange coupling observed in the ferromagnetic permalloy (Py)/(001) $BiFeO_3$ crystal. (a) and (b) A magnetic hysteresis loop taken along the [010] (a) and [100] (b) directions of the crystal showing a square hysteresis of an easy axis (a) and the large saturation field of the hard axis (b). (c) Schematic of the spin cycloid projected onto the Py/$BiFeO_3$ interface plane and propagates in the direction of $\vec{q}$. (d) The Py layer can minimize the Heizenberg exchange and demagnetization energies by "wiggling" in phase with the oscillation of the spin cycloid and ordering the moments along the cycloid propagation direction. (e) A high-energy state when the net magnetization of Py is orthogonal to the spin cycloid propagation direction, indicating a strong uniaxial anisotropy should be observed. Reprinted with permission from Lebeugle *et al.*, Phys. Rev. Lett. **103**, 257601 (2009). Copyright 2009 American Physical Society.

domain walls) and a mosaic (primarily 109° domain walls) $BiFeO_3$ film, the magnitude of the exchange bias was found to scale with the length of the 109° domain walls while being independent of the length of the 71° domain walls (Fig. 4). The enhanced coercive field of the exchange coupled $Co_{0.90}Fe_{0.10}$ layer was independent of the domain wall flavor suggesting a coupling with the bulk of the domain. For both the 4-variant and a mosaic $BiFeO_3$ films, it was found that the direction of the uniaxial or unidirectional anisotropy is governed by the direction of the applied magnetic field during the growth of the $Co_{0.90}Fe_{0.10}$ layer and did not correlate with the domain structure. While the details of the spin structure in each of the domain walls are still ongoing investigation, it is interesting to note that signatures of magnetic order in the 109° domain wall have emerged in X-ray magnetic circular dichroism (XMCD) and magnetotransport measurements and remain absent for the 71° and 180° domain walls.[76]

3. Multidomain thin films: Effect of domain structure

The domain structure of $BiFeO_3$ is sensitive to the electrostatic and elastic boundary conditions and the deposition rate. Hence, the magnetic interface exchange coupling will be sensitive to the same conditions. The 4-variant and mosaic films grown on (001) $SrTiO_3$ (Figs. 4(a) and 4(b)), for example, are grown with different deposition rates but with otherwise similar deposition conditions. By changing the elastic boundary conditions from the isotropic $\sim -1.5\%$ strain imparted by an $SrTiO_3$ substrate to a small, anisotropic strain of -0.3% from a (110) $DyScO_3$ substrate a well-ordered, quasi-periodic, 2-variant, striped domain structure with solely 71° or 109° domain walls can be achieved[77] (see Fig. 5(c) for an IP PFM image the domain structure, no out-of-plane PFM image for the 71° striped sample is presented since it is a uniform contrast). This was a significant development since the study of the properties of domain walls and multiferroic domains require their formation be controlled.

In an exchange-coupled heterostructure, the anisotropy and domain structure of the anisotropically strained $BiFeO_3$ layer can be transferred to a TMF through exchange coupling. Figs. 5(a) and 5(b) show the angle dependent magnetic hysteresis loops from $Co_{0.90}Fe_{0.10}/BiFeO_3$ bilayers where the applied magnetic field during the growth of the TMF was applied (b) parallel and perpendicular (a) to the $BiFeO_3$ domain walls to test if the applied field or the multiferroic would govern the anisotropy of the system. Recall that in Refs. 48 and 70 the anisotropy direction is set by the applied magnetic field during the growth of the TMF. In Fig. 5, the domain walls are all 71° so that there is a net in-plane component of the ferroelectric polarization ($P_{net\ IP}$) that points perpendicular to the domain walls and the out-of-plane component is uniform across domains. Irrespective of the orientation of the growth field, the anisotropy is always uniaxial and along the axis corresponding to the direction of $P_{net\ IP}$. This trend was observed regardless of the orientation of the $BiFeO_3$ growth terraces with respect to the ferroelectric domain walls. These heterostructures show an enhancement of the coercive field, when compared to $Co_{0.90}Fe_{0.10}$ grown on a $DyScO_3$ substrate, and negligible unidirectional anisotropy.

The combination of XMCD with photoemission electron microscopy (PEEM) at the Co L_3–edge and PFM images shown in Fig. 5(c) show the strong correlation between the domain structures of the two layers. These images reveal that both layers are composed of a well-ordered array of long, striped domains with two variants of the relevant order parameter. A closer look into the regions outlined by blue

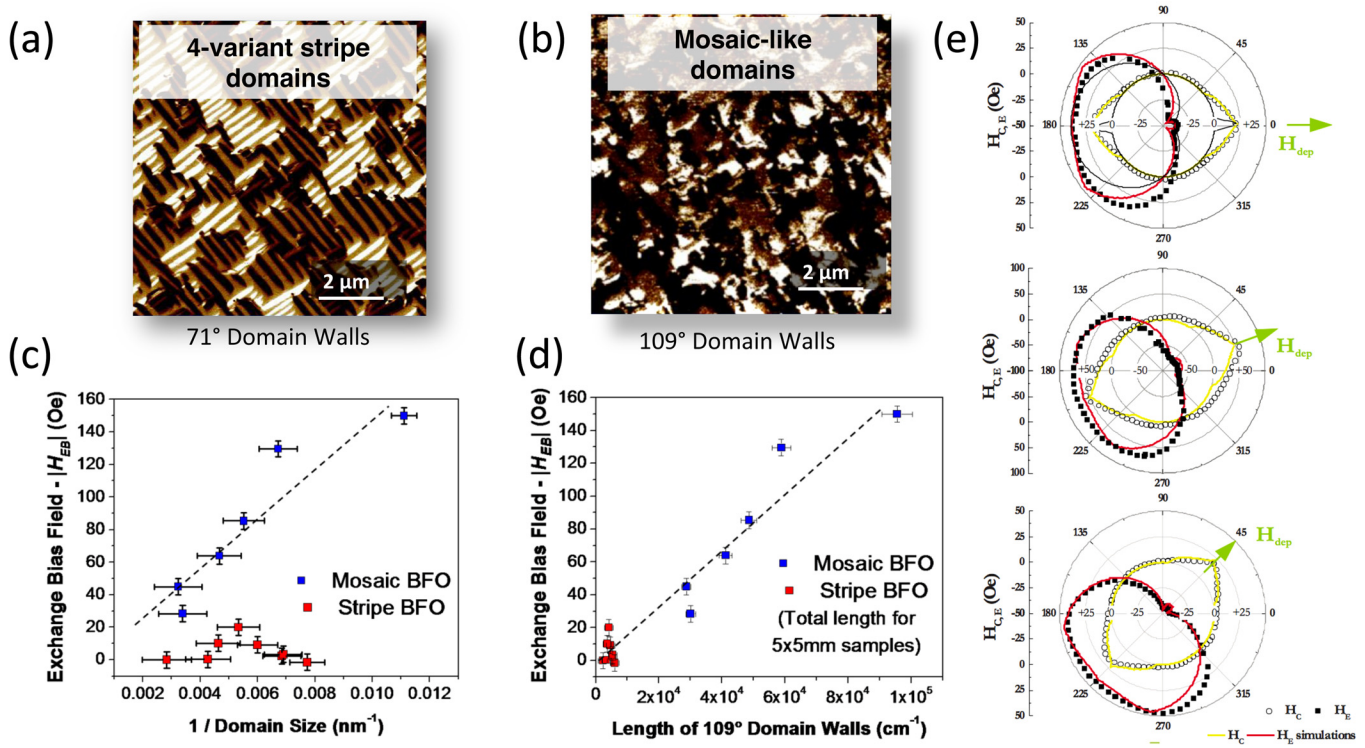

FIG. 4. (a) In-plane PFM image of a 4-variant striped domain $BiFeO_3$ film containing primarily 71° domain walls. (b) In-plane PFM image of a mosaic domain $BiFeO_3$ film containing primarily 109° domain walls. (c) Magnitude of the exchange bias field vs. the inverse of the domain size for the 4-variant and mosaic $BiFeO_3$ films. (d) Magnitude of the exchange bias field vs. the length of the 109° domain walls present in the 4-variant and mosaic $BiFeO_3$ films. (e) Polar plots illustrating that the applied magnetic field during the $Co_{0.90}Fe_{0.10}$ growth (H_{dep}) governs the direction of the anisotropy. Reprinted with permission from Martin *et al.*, Nano Lett. **8**, 2050 (2008). Copyright 2008 American Chemical Society. Reprinted with permission Lebeugle *et al.*, Phys. Rev. B **81**, 134411 (2010). Copyright 2010 American Physical Society.

boxes in Figs. 5(c) and 5(d) reveals a nearly one-to-one mapping of the multiferroic domain structure into the TMF, highlighted by the encircled "dislocation" structure. Furthermore, a collinear arrangement is observed between the in-plane projection of each polarization variant and the moment from the corresponding $Co_{0.90}Fe_{0.10}$ domain (arrows in the figure). One should caveat this conclusion with the following: the coupling is not between the in-plane projection of the polarization and the magnetic moment in the CoFe; instead, the coupling is between the in-plane projection of the canted moment in the BFO (which on this surface projects parallel to the polarization).

Employing the orthogonal relationship between $\vec{P}$, $\vec{L}$, and $\vec{M}_c$,[36] the orientations of these macroscopic order parameters in $BiFeO_3$ were determined through a combination of magnetometry, XMCD, and scanning probe measurements. With the orientations of these macroscopic order parameters determined, a mechanism of the exchange coupling was inferred. A schematic of the $Co_{0.90}Fe_{0.10}$/2-variant 71° striped $BiFeO_3$ structure with all of the relevant order parameters is given in Fig. 6. Within a single unit cell of $BiFeO_3$, with a polarization ($\vec{P}$) pointing along a ⟨111⟩ direction, the canted moment ($\vec{M}_c$) and the antiferromagnetic axis ($\vec{L}$) lie perpendicular to each other and in the (111) plane.[36] The magnetic hysteresis loops of the $Co_{0.90}Fe_{0.10}/BiFeO_3$ heterostructure presented in Figs. 5(a) and 5(b) suggest a strong coupling of the $Co_{0.90}Fe_{0.10}$ moments to the anisotropy of the $BiFeO_3$. To separate the convolution of a stress induced anisotropy and an exchange coupling driven anisotropy, a thin (1.5 nm), non-magnetic, and insulating $SrTiO_3$ layer was inserted between the $Co_{0.90}Fe_{0.10}$ and the $BiFeO_3$. The spacer acts to prevent any magnetic exchange between the layers since it is an interface driven effect, while the elastic interaction still transfers through the $SrTiO_3$. Magnetometry and XMCD measurements of the $Co_{0.90}Fe_{0.10}$/(1.5 nm) $SrTiO_3/BiFeO_3$ heterostructure show that the anisotropy of the $Co_{0.90}Fe_{0.10}$ is now governed by the direction of the applied growth field, the enhanced coercivity is quenched, and no correlation of the $Co_{0.90}Fe_{0.10}$ and $BiFeO_3$ domains was observed (not shown). These measurements provide the evidence that the coupling observed in the $Co_{0.90}Fe_{0.10}/BiFeO_3$ heterostructure is driven by magnetic interface exchange and not an effect of the elastic conditions. It should also be noted that the $Co_{0.90}Fe_{0.10}$ composition is intentional because of a vanishing magnetostriction coefficient ($\lambda_s \sim 10^{-7}$) observed in Co rich Co-Fe alloys.[78] X-ray magnetic linear dichroism (XMLD) PEEM measurements of both 4-variant and 2-variant striped $BiFeO_3$ films independently confirmed the orientation of the antiferromagnetic axis to lie in the (001) plane along a ⟨110⟩ type direction and perpendicular to the (001) projection of the ferroelectric polarization.[75] Thus, the one-to-one correlation between the direction of the magnetic moments within each $Co_{.90}Fe_{.10}$ domain and the ferroelectric polarization within each $BiFeO_3$ domain observed in Refs. 71 and 72, and Fig. 5(c) determine that the correlation is driven by the $BiFeO_3$ canted moment that points along the ⟨112⟩ and projects

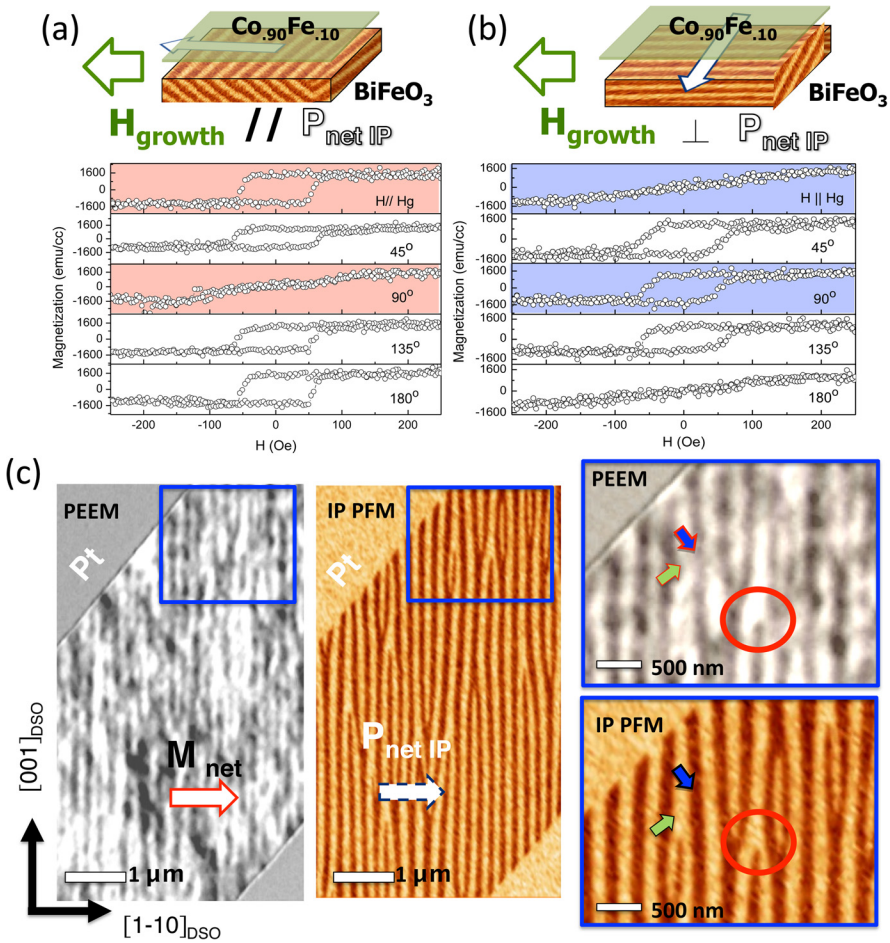

FIG. 5. Room temperature magnetic hysteresis loops obtained from $Co_{0.90}Fe_{0.10}$/2-variant $BiFeO_3$ where the growth field is applied (a) parallel to $P_{net\ IP}$ and (b) perpendicular to $P_{net\ IP}$. In either case, the easy axis is collinear with the direction of $P_{net\ IP}$. (c) XMCD-PEEM image taken at the Co edge (black and white image) of the $Co_{0.90}Fe_{0.10}$/2-variant striped $BiFeO_3$ heterostructure and an IP PFM image (brown and yellow image) of $BiFeO_3$ after the $Co_{0.90}Fe_{0.10}$ has been removed. The arrows in the XMCD images correspond to the direction of the net magnetization and the directions of the magnetizations associated with their respective domains. The arrows in the PFM images correspond to the direction of the net IP polarization and the IP direction (both variants have a component pointing into the page) of the polarization associated with their respective domains. Reprinted with permission from Heron *et al.*, Phys. Rev. Lett. **107**, 217202 (2011). Copyright 2011 American Physical Society.

parallel to the projected polarization on the (001) $BiFeO_3$ surface (Fig. 6).

The electric field control of magnetism is most easily envisioned through the electric field control of exchange bias since it breaks time reversal symmetry and manifests as an interfacial magnetic field.[79] Unfortunately, the 109° domain walls are metastable and revert to stable 71° domain walls after an electric field is applied, making a reversible process unlikely.[80,81] While the highly desirable exchange bias is absent in the films primarily consisting of 71° domain walls, a significant exchange coupling remains. This fact, along with the stability of 71° domain walls after an applied voltage make it a suitable system to study the electric field control of magnetism in exchange coupled multiferroic heterostructures.

B. Exchange coupling with oxide ferromagnets

A coherence of crystallinity across the interface of a $BiFeO_3$/crystalline oxide ferromagnet bilayer suggests expected differences in the interface exchange coupling due to ordered bonding. Additionally, there are significant intrinsic differences in the magnetism displayed by the ferromagnetic oxides. Magnetism in oxide ferromagnets emerges as a consequence of super- or double- exchange, display much smaller ordering temperatures and have significant magnetostriction coefficients compared to transition metal ferromagnets, and can display a magnetocrystalline anisotropy. Additionally, the correlations of the oxide ferromagnet give yet another mechanism by which unique interface phenomena can emerge, creating a platform for exploring the intriguing physics and opening the possibility for engineering functionalities. These points are exemplified in the studies of manganite $La_{0.7}Sr_{0.3}MnO_3$ (LSMO)/$BiFeO_3$ interfaces.

LSMO is a popular oxide ferromagnet due to its Curie temperature being near room temperature and the relative ease at which high quality epitaxial thin films can be deposited on other perovskite films and substrates. We note that there have been preliminary studies of exchange coupling between $BiFeO_3$ and other high Curie temperature oxide ferrimagnets (such as the ferrite spinels);[82] however, we highlight the results obtained from the LSMO/$BiFeO_3$ bilayer.

The LSMO/$BiFeO_3$ system has been used to demonstrate the electric field control of exchange bias at low temperature,[79,83] while a room temperature effect has remained a challenge. The root of this problem may lie in the correlated temperature dependence of the observed exchange bias, enhanced $BiFeO_3$ interface moment, and the interface orbital hybridization. These correlations suggest that an interface ferromagnetic ordering at the surface of $BiFeO_3$, and hence the exchange bias, can be attributed to an orbital reconstruction induced by the orbital ordering in the manganite film (see Fig. 7). Fig. 7(a) shows magnetization hysteresis loops of LSMO (red) and LSMO/$BiFeO_3$ films (blue and green) taken at 10 K. The LSMO/$BiFeO_3$ was cooled from high temperature under +1 T and −1 T to illustrate the negative exchange bias and the presence of pinned uncompensated spins at the

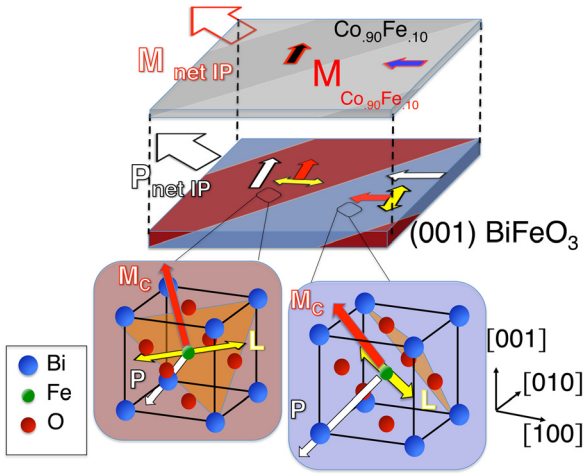

FIG. 6. A schematic illustration of the magnetic interface coupling in the $Co_{0.90}Fe_{0.10}$/2-variant striped $BiFeO_3$ heterostructure. Reprinted figure with permission from Heron *et al.*, Phys. Rev. Lett. **107**, 217202 (2011). Copyright 2011 American Physical Society.

$BiFeO_3$ interface and ferromagnetically coupled to the LSMO layer. A key feature of the exchange bias observed in the LSMO/$BiFeO_3$ system is the independence of the exchange bias on the ferroelectric domains, indicating a completely different mechanism of exchange coupling in this system than that observed in the TMF/$BiFeO_3$ system. Fig. 7(b) compares the Fe XMCD spectra from LSMO/$BiFeO_3$, $BiFeO_3$, and other Fe based compounds. A measurable Fe XMCD signal is obtained from the LSMO/$BiFeO_3$ bilayer, in stark contrast to the spectra obtained from a bare $BiFeO_3$ film; this indicates an enhanced interface moment. Figs. 7(c) and 7(d) illustrate the correlation between the enhanced moment measured in the Fe XMCD, the exchange bias, and the orbital reconstruction measured by x-ray absorption spectroscopy (XAS) at the oxygen-K edge. All three of the signals reach a steady state near 100 K.

The exchange bias, enhanced $BiFeO_3$ surface moment, and the orbital hybridization were described using an electronic hybridization model and the framework provided by the Goodenough-Kanamori-Anderson rules. Fig. 8(a) shows the proposed electronic hybridization at the LSMO/$BiFeO_3$ interface. The red shift of the $d_{3z^2-r^2}$ observed in the XAS temperature dependence (Fig. 7(d)) suggests a bonding state and anti-bonding state corresponding to this orbital after hybridization. Using this electronic configuration, the spin order is then inferred. The super-exchange interactions between the Fe^{3+} and $Mn^{3+\ (4+)}$ are ferromagnetic while the super-exchange interaction between the interface Mn and the bulk Mn in the LSMO layer is antiferromagnetic (Fig. 8(b)). Orbital ordering then leads to a competition between bulk

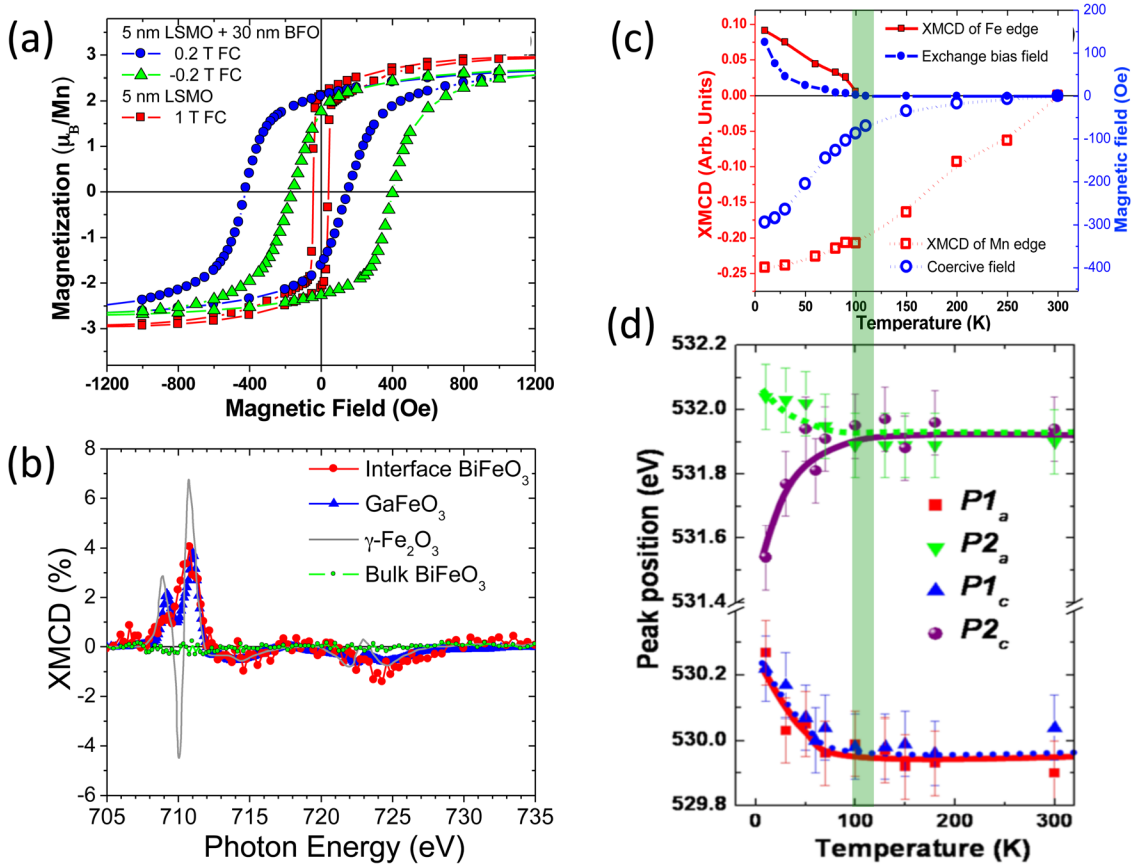

FIG. 7. (a) Magnetic hysteresis loops of LSMO (red) and LSMO/BFO (blue and green) films at 10 K illustrating the broadening of the hysteresis and the negative exchange bias in the LSMO/BFO bilayer. (b) XMCD spectra from a LSMO/BFO bilayer, $GaFeO_3$, γ-Fe_2O_3, and single-layer BFO films at 10 K. (c) and (d) Temperature dependent magnetometry and XAS measurements highlight a correlation of the exchange coupling, the ferromagnetic Fe moment, and the orbital reconstruction. The red shift of the $d_{3z^2-r^2}$ orbital ($P2_c$) indicates hybridization between Mn and Fe at the interface. Reprinted with permission from Yu *et al.*, Phys. Rev. Lett. **105**, 027201 (2010). Copyright 2010 American Physical Society.

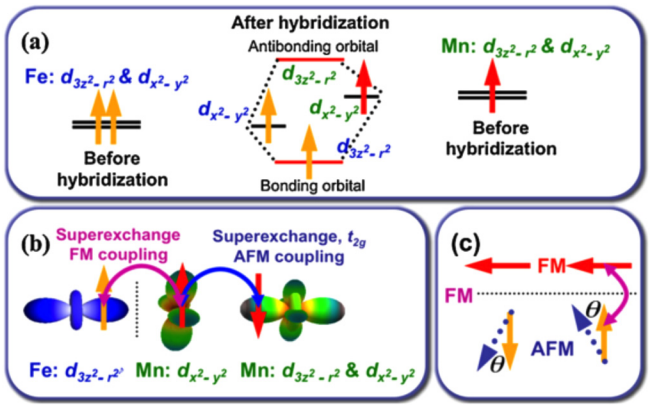

FIG. 8. (a) Schematic of the interface electronic orbital reconstruction with hybridization. (b) Proposed interface spin configuration and coupling mechanism with $d_{x^2-y^2}$ orbital ordering in the interfacial LSMO. (c) Schematic of the canting of the antiferromagnetic moments at the interface. Reprinted with permission from Yu *et al.*, Phys. Rev. Lett. **105**, 027201 (2010). Copyright 2010 American Physical Society.

antiferromagnetism and surface ferromagnetism in the $BiFeO_3$ layer. Fig. 8(c) schematically illustrates the significant canting of the $BiFeO_3$ magnetic structure induced from this competition between the bulk antiferromagnetic order and the induced ferromagnetic order due to the orbital ordering. Later, a more rigorous calculation employing a model Hamiltonian confirmed the experimental results and postulated that the competition of the ferromagnetic interaction and the bulk antiferromagnetic interaction drives the large surface canting.[84] Interestingly, the calculation of Ref. 84 predicts that the exchange coupling strength and sign (i.e., the canting magnitude and direction at the $BiFeO_3$ surface) are dependent on the interface charge density.

The exchange coupling in the aforementioned LSMO/$BiFeO_3$ bilayer is quite clearly driven by a different mechanism than that found for TMF/$BiFeO_3$ bilayers; however, because epitaxy is preserved in ferromagnetic oxide/$BiFeO_3$ heterostructures, the system can be engineered to yield similar magnetic properties to those observed in TMF/$BiFeO_3$ bilayers. Similar to the $Co_{0.90}Fe_{0.10}$/$BiFeO_3$ heterostructure, a 2-variant, striped $BiFeO_3$ film can induce a 2-variant, striped magnetic domain structure in the coupled LSMO layer which gives rise to a uniaxial anisotropy in the film. Figs. 9(a) and 9(b) show magnetic FM (MFM) and PFM images of the LSMO/$BiFeO_3$ and LSMO/$SrTiO_3$/$BiFeO_3$ systems, respectively. Even with the insertion of a thin, non-magnetic spacer layer ($SrTiO_3$), the LSMO layer adapts the 2-variant striped domain structure of the underlying $BiFeO_3$ film. The insertion of the thin non-magnetic spacer layer eliminates magnetic exchange coupling between the two layers while still allowing strain to transfer from the $BiFeO_3$ layer to the LSMO layer. Thus, the elongation of the $BiFeO_3$ unit cell (driven by the polarization) couples to the LSMO unit cell and the large, positive magnetostriction coefficient of LSMO[85,86] causes the moments to align with the elongation of the lattice. This coupling is fundamentally different from the one-to-one domain correlation observed in the $Co_{0.90}Fe_{0.10}$/$BiFeO_3$ system, where exchange coupling is the driving mechanism of the correlation.

In this section, we have highlighted some of the distinguishing characteristics of exchange coupling of an oxide ferro(ferri)magnet to multiferroic $BiFeO_3$. The coupling of the lattice opens pathways for new coupling phenomena that may be driven by correlations in the oxide ferro(ferri)magnet. We note that the results presented in Fig. 9 are not driven by a magnetic exchange with $BiFeO_3$ and do not require a multiferroic to achieve the 2-variant, striped domain structure. Since the coupling is driven by strain, the intrinsic magnetoelectric effect of $BiFeO_3$ is likely unnecessary for the electric field control of magnetism in this heterostructure, and, thus, is more akin to a traditional composite multiferroic. Nonetheless, these results highlight the fact that lattice coupling can enable alternate methods of coupling through which new coupling mechanisms maybe found and the magnetic properties of the system may be tailored.

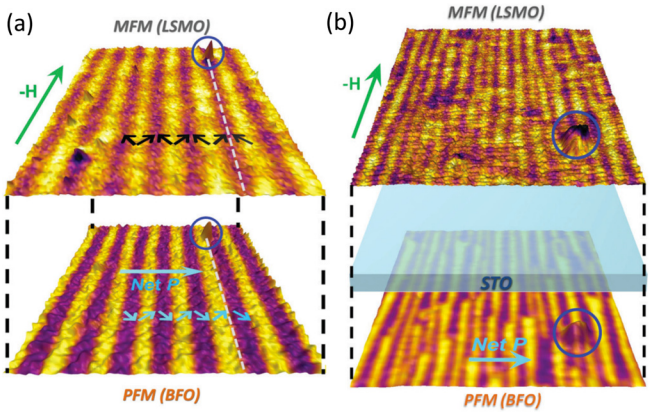

FIG. 9. (a) MFM image of LSMO/BFO laid over the PFM image of the $BiFeO_3$ film before LSMO deposition. (b) MFM of the LSMO/STO/$BiFeO_3$ multilayer and PFM of the $BiFeO_3$ layer before the deposition of LSMO/STO layers. There is a clear striped, magnetic domain structure in the LSMO correlated to the $BiFeO_3$ striped domains both with and without the insertion of the non-magnetic STO layer. Reprinted with permission from You *et al.*, Phys. Rev. B **88**, 184426 (2013). Copyright 2013 American Physical Society.

III. ELECTRIC FIELD CONTROL OF MAGNETISM

A. Electric field control of antiferromagnetism

The first milestone in the advancement of the electric field control of magnetism in exchange coupled $BiFeO_3$ based heterostructures was the experimental observation of the magnetoelectric effect at room temperature in $BiFeO_3$ films. The 2005 study by Zhao *et al.*, combined PFM and XMLD-PEEM to make several major discoveries.[75] (1) The antiferromagnetic domain structure and the ferroelectric domain structure were found to be coupled such that information on the size and order of antiferromagnetic domains can be determined through imaging the ferroelectric domain structure both before (Figs. 10(a) and 10(b)) and after (inside yellow dotted squares in Figs. 10(c) and 10(d)) electrical switching with an out-of-plane oriented electric field. (2) It confirmed that $BiFeO_3$ films are magnetoelectric at room temperature. (3) It was determined that only the 109° ferroelectric switching event underwent a magnetoelectric switching event. (4) The magnetoelectric switching was shown to be stable over long periods, i.e., is non-volatile. These

findings were later confirmed in bulk single crystals by neutron diffraction measurements.[87–89] The results in Ref. 75 were rationalized with the notion that the projection of the {111} magnetic plane onto the (001) plane only changes when the out-of-plane electric field drives a 109° ferroelectric switching event (see the schematics in Figs. 10(e)–10(h)).

B. Electric field control of exchange bias

The early attempts to establish the electric field control of an exchange-coupled ferromagnet in a multiferroic-based heterostructure were done with the vision of controlling the ferromagnetic layer through the exchange bias. Laukin *et al.* showed the first report of the electric field control of exchange bias at 2 K, in a Py/$YMnO_3$ heterostructure using a combination magnetometry and anisotropic magnetoresistance (AMR).[90] Using the temperature dependence of the exchange bias effect in this heterostructure, AMR curves with and without the influence of exchange bias could be taken. Then comparing these curves to AMR curves taken with $YMnO_3$ under an applied bias revealed a change in the exchange bias driven magnetic anisotropy.

It was not until 2010 that the reversible control and quantification of the modulations to the exchange bias through the applied voltage was demonstrated at 5.5 K.[79] Wu *et al.* fabricated devices with the LSMO/$BiFeO_3$ heterostructure where an out-of-plane electric field can be applied to the $BiFeO_3$ layer and the magnetic anisotropy of the LSMO layer could be monitored through magnetoresistance measurements (see Fig. 11). From the magnetoresistance curves, the magnitude and the direction of the exchange bias could be quantified. Bipolar voltage pulses were found to reversibly modulate the magnitude of the exchange coupling between two states, one with a near zero exchange field in a non-volatile way but the sign of the exchange bias was not found to reverse. Only recently could the sign of the exchange bias be reversed with an applied, bipolar electric field in this system. In the model of exchange bias at the LSMO/$BiFeO_3$ interface described in Sec. II B, the $BiFeO_3$ Fe^{3+} atoms are hybridized with the LSMO $Mn^{3+/4+}$ atoms. This hybridization drives the formation of an enhanced canted moment and the exchange bias. The reversal of the exchange bias is the attributed to the shift of the Fe^{3+} and Bi^{3+} ions in $BiFeO_3$ relative to the oxygen octahedral[91] and the surface when ferroelectric polarization is switched. The shift is proposed to alter the interaction between the surface Fe^{3+} atoms and $Mn^{3+/4+}$ atoms, thereby altering the exchange bias.

Advances toward the reversible electric field control of exchange bias at room temperature in a ferromagnet/$BiFeO_3$ bilayer have been difficult. The current issues stem from the mechanism of exchange coupling. Either the blocking temperature is much lower than room temperature regardless of the ferromagnet's much higher Curie temperature, as is the case for LSMO/$BiFeO_3$ ($T_{blocking} \sim 100$ K (Fig. 7(c)), $T_C \sim 350$ K) or the exchange bias is driven by the metastable 109° domain walls; hence, the exchange bias decreases significantly and irreversibly with every applied voltage pulse.[80] This issue may be solved if a new mechanism for driving exchange bias is discovered, another ferromagnetic layer with stronger correlations then LSMO is coupled, or if the $BiFeO_3$ can be engineered to pin or stabilize the 109° domain walls.

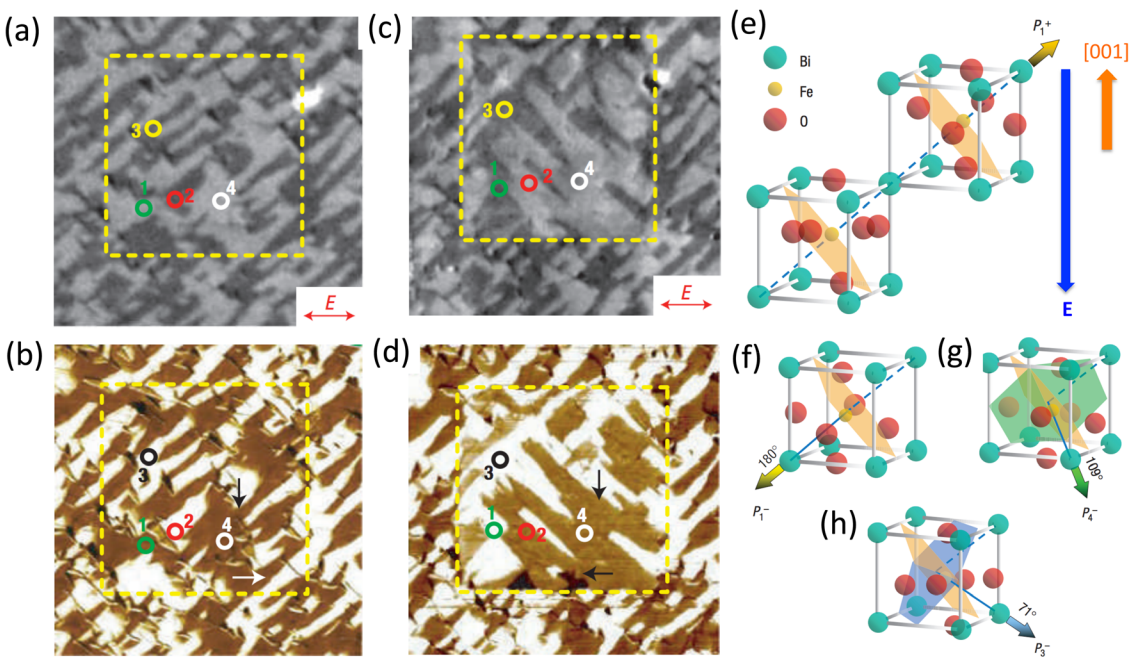

FIG. 10. XMLD-PEEM (a) and PFM (b) of a $BiFeO_3$ film before electrical switching. The yellow dotted box indicates where electrical switching will occur. The double-headed red arrow indicates the axis of polarization for the incoming X-rays. The corresponding XMLD-PEEM (c) and PFM (d) after electrical switching. A 109° ferroelectric switching event occurred at regions 1 and 2 while regions 3 and 4 underwent 71° and 180° ferroelectric switching events. No change in the XMLD contrast is observed for the 71° and 180° ferroelectric switching events. Illustrations of the polarization and magnetic plane are shown for the (f) 180°, (g) 109°, and (h) 71° rotations of the polarization in $BiFeO_3$ unit cells. Reprinted with permission from Zhao *et al.*, Nature Mater. **5**, 823 (2006). Copyright 2006 Zhao *et al.*

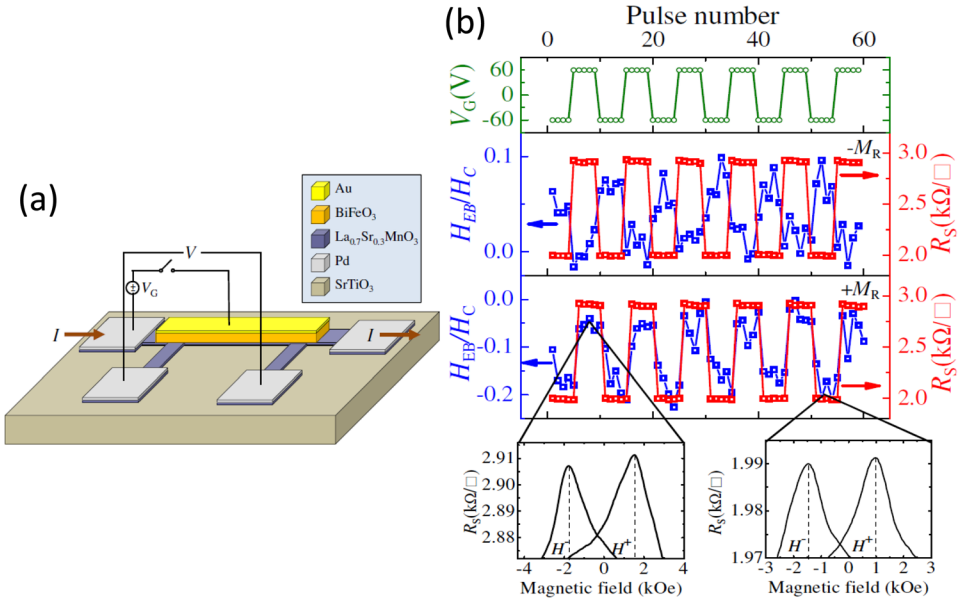

FIG. 11. (a) A device schematic of the device used to quantify changes in the electric field induced modulation of exchange bias at the LSMO/$BiFeO_3$. (b) The voltage pulse sequence, the modulation of exchange bias at 5.5 K with the LSMO magnetization in the negative ($-M_R$) and positive ($+M_R$) remnant states, and examples of the magnetoresistance curves used to quantify the exchange bias field (H_{EB}) and the coercive field (H_C). Reprinted with permission from Wu *et al.*, Nature Mater. **9**, 756 (2010). Copyright 2010 Wu *et al.*

C. Electric field control of magnetization direction without exchange bias

The electric field control of magnetism without the electric field control of exchange bias is not expected to reverse the direction of the coupled magnetization by symmetry. Since both the electric field and the polarization break space inversion symmetry and in the absence of exchange bias, there is no time reversal symmetry-breaking stimulus that can reverse a magnetization. Nonetheless, the magnetic anisotropy and magnetization direction can be controlled via an applied electric field. We have already highlighted the differences in coupling between a TMF to $BiFeO_3$ single domain bulk crystals and multidomain thin films where exchange coupling is not observed with the distinctions residing in the magnetic state of the canted moment (i.e., a spin cycloid that propagates in the ⟨110⟩ type directions or a long range moment that projects parallel to the polarization on the (001) surface). In this section, we will discuss the works that demonstrate the electric field control of a TMF in contact with both $BiFeO_3$ bulk crystals and multidomain thin films with only an applied electric field at room temperature. Furthermore, we note that engineering the domain structure of the films can lead to the situation where a net magnetization can reverse with the applied electric field while the laws of symmetry are obeyed.

D. Electric field control with single domain $BiFeO_3$ crystals

Lebeugle *et al.* described the exchange coupling of a TMF with $BiFeO_3$ crystals, as well as the electric field control of these exchange coupled spins.[69] Using a combination of optical techniques, the ferroelectric domains (it should be noted that $BiFeO_3$ crystals are not truly single domain, however, due to the very large domain size in crystals the domain wall density is not significant) and ferromagnetic domains could be imaged and magnetic hysteresis loops could be measured. Taking an angular set of magnetic hysteresis loops, the evolution of the systems magnetic anisotropy after the application of an electric field could be observed (Figs. 12(a) and 12(b)). The regions of the crystal that had experienced a 90° change in the direction of the polarization also experienced a 90° change in the direction of the magnetic anisotropy. The anisotropy remained uniaxial after the electrical switching. While a reversal of the magnetization was not observed, this work highlights that exchange bias is not required for the electric field control of magnetic anisotropy. A correlation between the ferroelectric and ferromagnetic domains persisted after the application of the electric field. The effect was observed to be reversible, however, after just five cycles the domain correlation was broken. They postulate that the correlation breaks down due to the non-uniqueness of the spin cycloid propagation direction for a given polarization. Since each polarization has three possible directions for the spin cycloid to propagate, there exist shared propagation directions among the eight possible polarization directions.[88,89] Thus, the spin cycloid is not always required to change direction upon switching the polarization; indeed, it can be a detriment.

E. Electric field control with multidomain $BiFeO_3$ thin films

The observation of the electric field control of the antiferromagnetism in $BiFeO_3$ thin films[75] sets the stage for the electric field control of a ferromagnetic layer exchange coupled to the $BiFeO_3$ film. In the seminal paper by Chu *et al.*, the magnetic anisotropy of small magnetic features ($2 \times 6\ \mu m^2$ $Co_{0.90}Fe_{0.10}$ dot) were reversibly toggled by an in-plane electric field (see Fig. 13).[92] This was another demonstration of a new room temperature functionality employing this materials system. Furthermore, these researchers demonstrated that the electric field control can be exchange mediated without exchange bias, was reversible and non-volatile, and, most importantly, showed that the in-plane switching of a polarization by 71° is a magnetoelectric switch. Prior to this only the out-of-plane 109° switch was known to be magnetoelectric.[75]

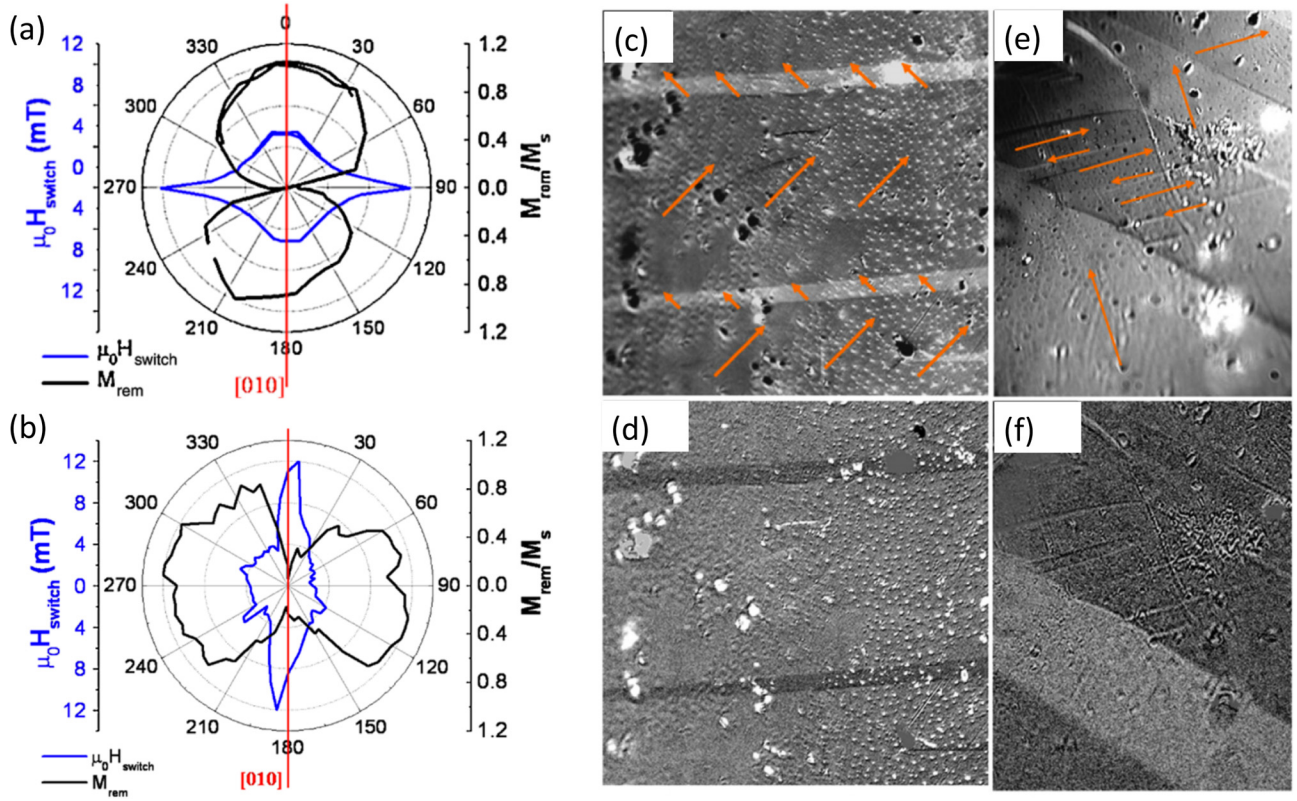

FIG. 12. (a) and (b) Polar plots illustrating the magnetic anisotropy of the Py/$BiFeO_3$ bulk crystal before (a) and after (b) the application of an electric field. For the regions of the crystal that experienced a 90° switch of the polarization from the applied electric field, the magnetic anisotropy has also rotated 90°. Ferroelectric (c) and magnetic (d) domain structures after the first application of the electric field. Ferroelectric (e) and magnetic (f) domain structures after the fifth application of the electric field. The domain correlation is broken in these images, as can be seen by the magnetic domain wall in the lower left-hand corner of (f). Orange arrows give the direction of the ferroelectric polarization. Reprinted figure with permission from Lebeugle *et al.*, Phys. Rev. Lett. **103**, 257601 (2009). Copyright 2009 American Physical Society.

To probe the ability to electrically control the ferromagnetic state of the $Co_{0.90}Fe_{0.10}$ layer, the heterostructures of $Co_{0.90}Fe_{0.10}$/4-variant $BiFeO_3$ were grown on pre-patterned substrates with conducting $SrRuO_3$ (SRO) interdigitated electrodes. The poling structure was carefully designed to ensure the 71° ferroelectric switching event by rotating the electrodes to be 45° from the domain walls (Fig. 13).[93] The switching event was found to rotate the domain ferroelectric wall orientation by 90° from switch to switch. Similarly, XMCD images of the exchange coupled $Co_{0.90}Fe_{0.10}$ layer also show a rotation of the ferromagnetic domain wall orientation from switch to switch, in agreement with the ferroelectric switching and indicating some correlation of domain structure.

The possible domain correlation observed in Fig. 13 using the $Co_{0.90}Fe_{0.10}$/4-variant $BiFeO_3$ and the successful demonstration of the electric field control of the magnetization at room temperature in this system motivate a similar study with the $Co_{0.90}Fe_{0.10}$/2-variant $BiFeO_3$ heterostructure. Since only the out-of-plane 109° and the in-plane 71° ferroelectric switches have been found to be magnetoelectric, a careful consideration of the ferroelectric switching in 2-variant $BiFeO_3$ is needed for the electric field control of magnetism. In 2-variant $BiFeO_3$, the net in-plane polarization can be reversed with only the in-plane components contributing to the total switching of the polarization.[71,94,95] A continuity of the domain walls across switched and unswitched regions illustrate that the domain switching is accomplished by 90° rotation of the in-plane polarization (in-plane 71° switch of the polarization vector) without creating additional domain walls (Figs. 14(a)–14(d)). Consistent with previous phase-field simulations of $BiFeO_3$,[96,97] the coercive field of

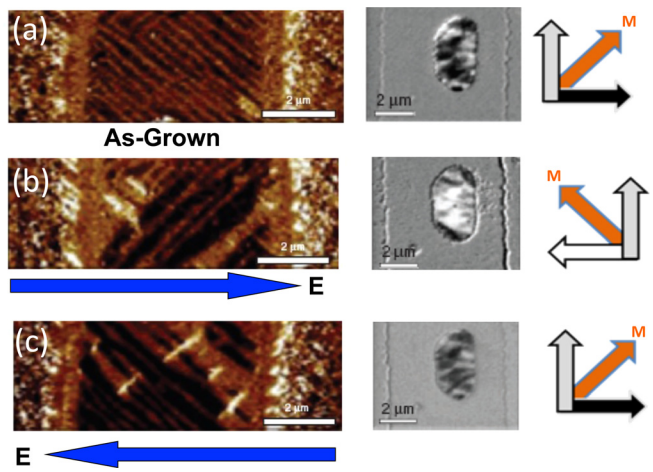

FIG. 13. In-plane PFM of the $BiFeO_3$ domain structure (left) and XMCD of a $Co_{0.90}Fe_{0.10}$ feature (middle) in a device architecture where an in-plane electric field can be applied (blue arrows). $BiFeO_3$ and the coupled $Co_{0.90}Fe_{0.10}$ feature are as-grown (a), 1st switch (b) and 2nd switch (c) states. (b) Schematics illustrating the correlation of XMCD contrast to moment direction and the direction of the total moment (orange arrow). Reprinted with permission from Chu *et al.*, Nature Mater. **7**, 478 (2008). Copyright 2008 Chu *et al.*

the 71° switch is then expected to be significantly lower than the 109° switch (in-plane 180°). Phase-field modeling has confirmed the switching mode as a mode of charge driven domain switching (a case where a large build up of charge at the domain walls drives ferroelectric switching due to only one of the two polarization variants switching under the applied electric field).[71,98] It was also determined that this mode of polarization switching is dependent on the strength of the applied electric field. If the field is large enough to drive the 109° switch in a domain, both the domain walls, along with the net in-plane polarization, rotate 90° as observed in Refs. 92 and 93. The unique one-to-one coupling of domain structure and collinear alignment of the in-plane polarization and the magnetization observed in the $Co_{0.90}Fe_{0.10}$/2-variant $BiFeO_3$ heterostructure (Fig. 5) suggests the reversal of the net in-plane polarization should lead to the reversal of the net $Co_{0.90}Fe_{0.10}$ magnetization.

Researchers had then undertaken the task of demonstrating an electric field induced stable reversal of a net magnetization at 300 K. Devices were designed to meet fundamental compatibility requirements for microelectronics by measuring the state of the device with a resistance measurement rather than a more complex optical measurement (Fig. 14(e)). The AMR of the $Co_{0.90}Fe_{0.10}$ was measured in the as-grown state and after subsequent electrical poling of the $BiFeO_3$ (Fig. 14(f)). The AMR is taken with an applied magnetic field that is smaller than the coercive field of the device to avoid switching but to allow the magnetization to wiggle about its anisotropy direction allowing the magnetization direction to be determined.[99,100] The phase of the AMR curves changes by 180° after each subsequent application of an electric field revealing a magnetization reversal and corroborates with the observation of the reversal of the net in-plane polarization after each application of the electric field. While this work demonstrated that anisotropy engineering leads to the unique exchange coupling and ferroelectric switching enables the voltage driven net magnetization reversal, it also highlights several issues that need to be tackled in the pursuit of a "real world" device application. Establishing such a reversal with the electric field applied out-of-plane (through the film thickness ~100 nm) could enable single digit switching voltages (200 V were used in Ref. 92 and 70 V in Ref. 71) and bring the energy consumption per unit area per switch below that of STT and into the realm of 100s of $\mu J/cm^2$ while simultaneously using an architecture better suited to achieve high device density. In the spirit of achieving higher device density, the devices should be scaled down to the sizes of modern magnetic bits (~180 nm × 70 nm), of course this would put the device within a single multiferroic domain raising a slew of new and old questions and concerns. These are just a few of the challenges that remain open for near future investigations and is the topic for Sec. IV.

IV. WHAT ARE THE ISSUES?: CHALLENGES AND FUTURE DIRECTIONS

Transitioning fundamental discoveries to real products is a monumental challenge. While there is still a long road to travel before a ferromagnetic/multiferroic heterostructure will impact technology, the works reviewed herein have illustrated the relevant parameters governing the interface coupling and the switching of the multiferroic. It is now time for researchers to use these tools to demonstrate a potential for technological impact. Here we discuss a small list of perhaps the most relevant challenges where future research initiatives must focus before circuit engineers can take a closer look at this materials system.

A. Magnetoelectric switching with an out-of-plane electric field

While the voltage control of a magnetization was shown in bilayers with $BiFeO_3$, the voltages required are too large for conventional microelectronics circuitry.[71,92] This detriment is due to the large in-plane electrode structures used in these early experiments; however, the geometries of these device structures were carefully chosen to drive the magnetoelectric in-plane 71° switching event which is responsible for the electric field induced rotation of the ferromagnetic moment. Naturally, a higher density of devices and lower switching voltages can be reached if a geometry employing an out-of-plane electric field is employed as the separation between electrodes then decreases from ~6 μm to ~100 nm.

Of more relevance is the magnetoelectric switching that can be controllably accessed with the application of an out-of-plane electric field for the deterministic control of a magnetization. For such an endeavor, it is important to consider the configuration of the system. The magnetization of a transition metal alloy ferromagnet will typically lie in the plane of the film due to the demagnetization energy. Hence, an in-plane rotation of the ferromagnetic moments is expected to occur when the magnetic plane of $BiFeO_3$ undergoes an in-plane rotation. This point illustrates the motivation to drive the in-plane 71° switching event in the early device structures. The 71° switch drives an in-plane rotation of the magnetic plane (Fig. 15(a)) and can be deterministically switched with an in-plane electrode geometry with the electrodes oriented 45° from the axis of the domain walls (Fig. 13). Now, considering a (001) oriented $BiFeO_3$ film, a vertically applied electric field must rotate the polarization by 71°, 109°, or 180° with each reversing the vertical component of the polarization (Fig. 15(a)). Of these, only the 109° and 180° rotate the in-plane component of the polarization and only the 109° drives an in-plane rotation of the magnetic plane (Fig. 15(a)). From a symmetry perspective, the DM vector $\vec{D}$ in $BiFeO_3$ is independent of the sign of the polar distortion (i.e., the polarization), rather it is dependent on the non-polar rotations of the network of oxygen octahedra.[43] This invariance can be overcome in the $R3c$ perovskite structure when the magnetic cations are situated on the A-site, which then leads to the DM interaction being induced by the polar distortion.[43] Nevertheless, the 180° switch in $BiFeO_3$ is expected to leave the magnetic plane invariant and, thus, is not magnetoelectric. This latter fact makes finding a mechanism for deterministically reversing a magnetization (the most desired outcome for conventional spintronics applications) by either in-plane or out-of-plane electric fields in this system even more challenging. Zhao *et al.* have demonstrated that an out-of-plane

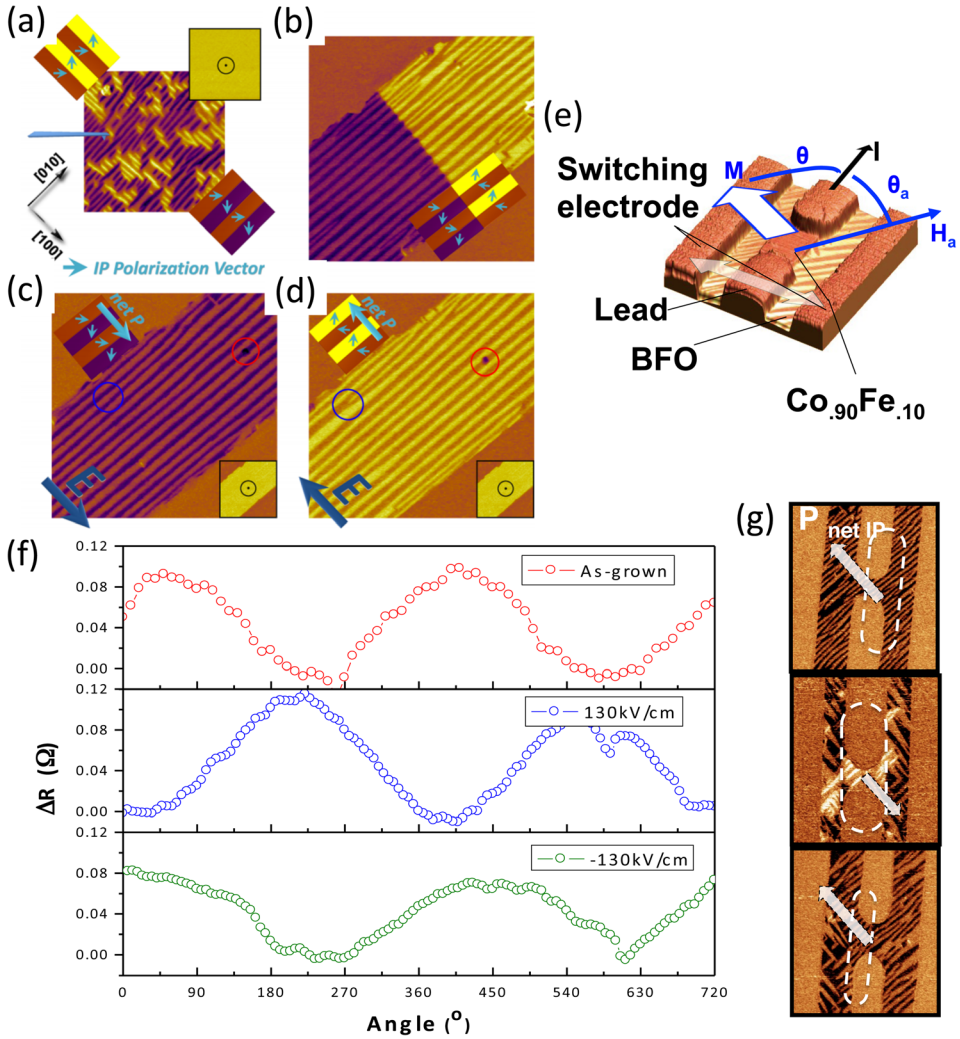

FIG. 14. (a) In-plane PFM of a 4-variant $BiFeO_3$ film and schematics illustrating the 4 polarization variants. The out-of-plane image is also included. (b) Partial switching of a pre-switched region of the capacitor. Pre-switching poles the state into a 2-variant film. Continuity of the domain walls is satisfied across the boundary and reveals that each polarization variant rotates 71° (90° in projection). (c) Saturated switching reverses the net in-plane polarization. (d) Reversible switching of the net in-plane polarization switched. (e) A combined image from AFM and PFM images highlighting the features of the magnetoelectric device and the configuration of the AMR measurements. The IP electric field is applied to the device via the two outer switching electrodes and the AMR is measured with a current flowing down the centrals leads to a $Co_{0.90}Fe_{0.10}$ dot. The sample is rotated in a small magnetic field ($H_a = 20$ Oe) to make the magnetization wiggle about its anisotropy direction. (f) AMR curves as a function of applied electric field. The phase of the AMR curves changes by 180° with respect to the previous curve after the application of the voltage pulse indicating a net magnetization reversal. (g) PFM of 3 devices in the states corresponding to the states in (f) but after the $Co_{0.90}Fe_{0.10}$ has been removed with a soft Ar ion milling. The net IP polarization reverses under the $Co_{0.90}Fe_{0.10}$ dot after every switching event. Reprinted with permission Heron *et al.*, Phys. Rev. Lett. **107**, 217202 (2011). Copyright 2011 American Physical Society. Reprinted with permission from Appl. Phys. Lett. **97**, 062910 (2010). Copyright 2010 AIP Publishing LLC.

electric field applied to a 4-variant (001) $BiFeO_3$ film can drives the out-of-plane 71°, 109°, and 180° ferroelectric switching events, however, it is only the out-of-plane 109° rotates the antiferromagnetic axis on the (001) surface.[75] Further investigation is needed to determine if the out-of-plane 109° switching event can be isolated from the out-of-plane 71° and 180° ferroelectric switching events in a vertical capacitor geometry and if then a coupled magnetization can then be rotated with an applied electric field. Thus, it is clear that a full understanding of the atomistics pathways for polarization switching needs to be understood; how this impacts the canted moment (i.e., the canted moment switches or doesn't) should indeed be explored.

Further consideration of the out-of-plane magnetoelectric switching possibilities must examine the activation barriers for each of the ferroelectric switching events and their dependence on elastic interactions with the underlying substrate and the $BiFeO_3$ matrix. Baek *et al.* have calculated that a 180° rotation of the polarization may occur through the combination of 71° and 109° rotations driven by the action of the electric field and the elastic interactions with the surrounding unswitched $BiFeO_3$ matrix.[96] Such a method of "combinatorial" switching could lead to a reversal of a magnetization circumventing the issue of magnetic invariance. Of course, other surface orientations of $BiFeO_3$ (such as the (011) and (111)) should be considered and could reveal unique switching pathways and magnetoelectric switching events. It is clear that theoretical and experimental investigations of the switching events in an out-of-plane capacitor structure are still needed to determine the feasibility

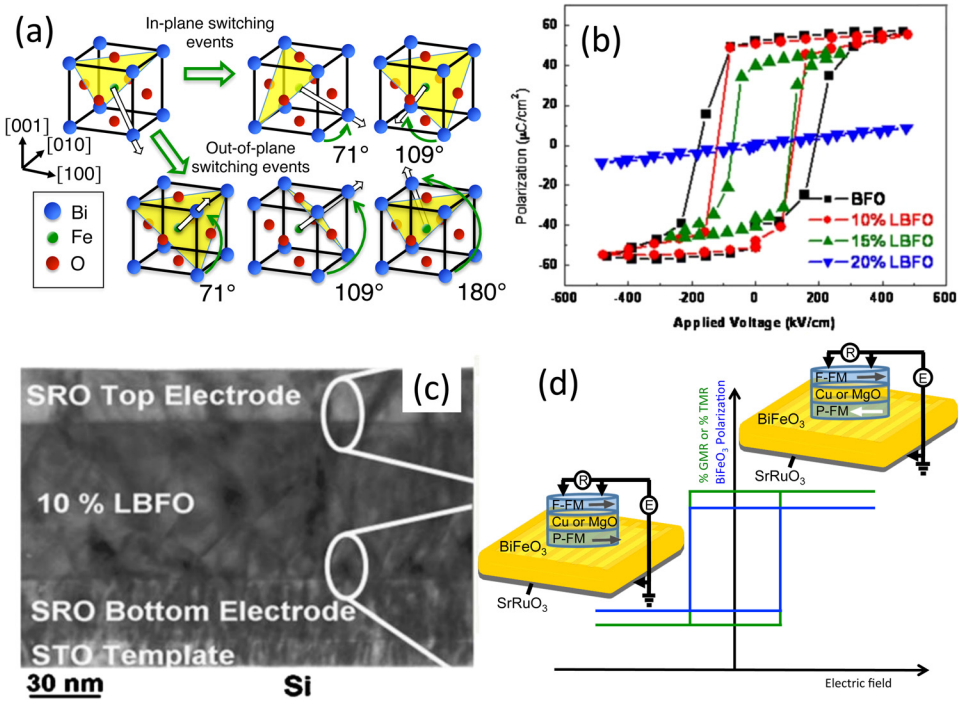

FIG. 15. (a) Illustrations of the magnetoelectric switching events possible in the $BiFeO_3$ system. The white arrows give the direction of the ⟨111⟩ oriented polarization. The (111) oriented magnetic plane is orthogonal to the polarization and is shown in yellow. An externally applied electric field directed in-plane (along the [110] or the [−110]) will lead to either a 71° or 109° in-plane switching event. A [001] oriented electric field can induce 71°, 109°, or a 180° out-of-plane switching events. The 180° switching event leaves the (111) magnetic plane invariant. (b) Ferroelectric hysteresis loops of $La_xBi_{1-x}FeO_3$ (where $x = 0$, 10, 15, and 20). (c) Cross-sectional TEM image of the SRO/$La_{0.10}Bi_{0.90}FeO_3$/SRO/STO/Si multilayer. (d) Schematic of a possible magnetoelectric magnetic multilayer device using $BiFeO_3$. The state of the device is written with an applied electric field to drive a magnetoelectric switching in the multiferroic, reversing the magnetization of the pinned ferromagnetic layer (P-FM) and keeping the free layer (F-FM) fixed. The reversal of the ferromagnetic layer switches the resistance state of the spin valve or magnetic tunnel junction into either a high or low resistance state depending on the relative orientations of the two ferromagnetic layers. Reprinted with permission from Appl. Phys. Lett. **92**, 102909 (2008). Copyright 2008 AIP Publishing LLC.

of a deterministic and reversible magnetoelectric switching event. It will then be up to researchers to determine if such a magnetoelectric switching occurs and if it can be harnessed in an exchange coupled heterostructure.

Pathways toward reduced energy consumption exist beyond moving to an out-of-plane device geometry. The ferroelectric properties of $BiFeO_3$ can be tuned, without significant changes in the magnetic properties, through chemical doping of the Bi site. Previous reports have shown that the substitution of 10 % La can reduce the switching to below 1 V for a ∼100 nm thick film.[101] There exist, however, fundamental limits to which the thickness of the $BiFeO_3$ can be scaled for these devices. While the ferroelectricity can exist down to very small scales (2–3 nm),[102] the exchange bias field of a CoFeB/$BiFeO_3$ heterostructure begins to sharply drop near 30 nm indicating a suppression of the antiferromagnetic Néel temperature.[70] If even lower energy consumption is required, materials engineering may be required to reduce the switching voltage further.

B. Integration with silicon

To pose a technological impact the next generation devices require compatibility with current CMOS technology. One of the key requisites is the epitaxial integration of $BiFeO_3$ with silicon. A significant materials advancement was made when $SrTiO_3$ buffer layers could be grown on silicon.[103,104] $SrTiO_3$ has become the workhorse of complex oxide thin film growth due to its cubic perovskite crystal structure and lattice constant that is relatively well matched to many other perovskites. Thus this discovery enables the integration of the correlated complex oxides that display the multi-functionality desired in next generation devices to be integrated with silicon based technology. Chu *et al.* have demonstrated the successful growth of $La_xBi_{1-x}FeO_3$ (where $x = 0$, 10, 15, and 20) on the $SrTiO_3$-templated silicon and with a conducting bottom electrode ($SrRuO_3$) for investigating the ferroelectric properties (Fig. 15(c)).[101] While the macroscopic ferroelectric properties of the un-doped films remain largely similar to those observed for the mosaic domain structure obtainable on $SrTiO_3$ substrates there is no report to whether the domain structure can be controlled through deposition conditions or other means. This is quite a significant research direction since the 4-variant and 2-variant stripe-like domain structures are the ones that have enabled the electrically controlled ferromagnetic layer. As we will discuss later, perhaps a single domain film is the most ideal.

C. Electrically controlled magnetic memory or logic element

While the spintronics community has been intrigued with the idea of electric field controlled spintronic devices, there still has yet to be a demonstration of a reversible and deterministic electric field control of such devices at room temperature using exchange-coupled multiferroic

heterostructure. While using current induced magnetic switching allows high memory densities, the present state-of-the-art devices are still energetically costly. We discussed the energy cost of an STT memory element in the introduction. Furthermore, the electric field control of ferromagnetism shown in Fig. 13 had come with a proposal for a magnetoelectric magnetic multilayer device that combines the advantages of ferroelectric (fast, low-power writing/switching) and ferromagnetic (non-volatility, easy readout of device state) memories (Fig. 15(d)). The resistance state of such a device is controlled using the magnetoelectrically pinned layer as the active layer rather than the low magnetic anisotropy free layer. The next step is to demonstrate such a device with a reversible switching of the resistance state using a multiferroic-spin valve ($BiFeO_3$/ferromagnet/Cu/ferromagnet) or multiferroic-tunnel junction ($BiFeO_3$/ferromagnet/MgO/ferromagnet) device with solely an electric field at room temperature.

When discussing such memory elements, it is important to consider the scale of modern devices. The size of a modern STT memory element is nearly a 60–70 nm × 180 nm, which is then capable of fitting within a single $BiFeO_3$ domain. Many of the basic questions remain unanswered when we consider the exchange coupling, ferroelectric switching, and magnetoelectric switching at these small scales.

D. Fatigue and reliability

References 69, 71, and 92 are three independent reports of the room temperature electric field control of a large magnetization in a TMF-$BiFeO_3$ heterostructure, however, these reports have also highlighted a significant lack of switching reliability. For the case of Py/$BiFeO_3$ single crystals, it was shown that after five cycles, regions where a correlated domain structure was observed were broken and these regions no longer switched under the applied electric field.[69] The lack of deterministic switching was explained through the degeneracy of the spin cycloid propagation direction with polarization direction. In the case of the $Co_{0.90}Fe_{0.10}/BiFeO_3$ thin film heterostructures the reliability numbers are even worse. No report has shown more than one complete switching cycle. While neither Ref. 71 nor 92 propose a mechanism of failure, Couet *et al.* have proposed and supported the argument that stems from the issue that has plagued applications with ferroelectrics, such as ferroelectric memories, for decades: the motion of ionic species (such as oxygen vacancies) under the large electric field and their trapping at the ferroelectric/metal electrode interface. Couet *et al.* investigated the interface chemistry and magnetism in Fe/$BaTiO_3$ and Fe/$LiNbO_3$ heterostructures as a function of an applied electric field.[105] It was determined that the Fe at the interface would oxidize as a threshold electric field is surpassed, creating a magnetically dead layer and irreversibly altering the magnetoelectric effect initially observed in these systems. They propose that the interdiffusion is largely driven by the amplification of the applied electric field by the large permittivity of the ferroelectric layer.[105] Additionally, they find that for a 300 kV/m electric field, 1.2 nm–2 nm of the Fe has oxidized. As the electric fields applied in Refs. 71 and 92 are on the order of 10 MV/m and Co is more easily oxidized than Fe, it seems plausible that the oxidation of the interface and breaking of the exchange coupling in $Co_{0.90}Fe_{0.10}/BiFeO_3$ heterostructures could happen over a few voltage pulses. Perhaps tailoring of the ferroelectric properties, possibly through La doping, to reduce the dielectric constant and reduce the electric field required for switching will improve device reliability.

The solution to polarization fatigue lies in the use of oxide switching electrodes[106] as the mobile ionic species can diffuse beyond the interface. Ultimately, this has lead to commercially viable, reliable ferroelectric memory technology. This suggests that the magnetoelectric switching of the heterostructure could be made robust to with an oxide as the ferromagnetic layer. As shown in Fig. 11(b) and Ref. 79, the LSMO/$BiFeO_3$ devices were shown to have been cycled five times with the claim of up to sixty cycles, however, room temperature functionality in this system has yet to be demonstrated.

V. SUMMARY

In this manuscript, we have reviewed the electric field control of magnetism using the ferromagnet/$BiFeO_3$ exchange coupled heterostructure. It is our hope that we have captured all of the excitement and nuances that have been used recently in this pursuit. The works presented herein have outlined the complexity of such an undertaking. While globally the route to the electric field control of magnetism in these heterostructures amounts to an understanding or engineering of the exchange coupling between the layers and the magnetoelectric switching of $BiFeO_3$, it is apparent that this requires an understanding of the chemical and physical changes that can occur at the interface and the relation of these interface energies to volumetric interaction energies. We have presented challenges that currently stand in the way for these advancements to impact technology, highlighting the importance of length scales and materials chemistry. We hope that this review of the achievements and challenges for $BiFeO_3$ based spintronics will motivate and aid the community to turn these challenges into accomplishments and lead to the adoption of the technology by circuit designers.

ACKNOWLEDGMENTS

J.T.H. acknowledges that this research was made with government support awarded by DOD, Air Force Office of Scientific Research, National Defense Science and Engineering Graduate (NDSEG) Fellowship, 32 CFR 168a. We thank C. M. Brooks and H. Nair for their comments on this manuscript. The authors recognize that this material is based upon work supported by the National Science Foundation (Nanosystems Engineering Research Center for Translational Applications of Nanoscale Multiferroic Systems) under Grant Number EEC-1160504 and the D.O.D.-A.R.O. M.U.R.I supported by the Army Research Office through Agreement Number W911NF-08-2-0032. R.R. acknowledges the support of the Director, Office of Basic Energy Sciences, Materials Science Division of the US Department of Energy under Contract Number

DE-AC02-05CH11231, the NSF MRSEC (DMR-00-80008), the Center for Energy Efficient Electronics Science (NSF Grant Number 0939514), the Western Institute of Nanoelectronics program, the STARnet FAME, as well as significant intellectual and financial support from scientists and engineers at Intel (e.g. Dmitri Nikonov). Finally, we would like to express our appreciation to all of the collaborators and coauthors for the work presented herein, specifically K. Ashraf, Y.-H. Chu, R. Dynes, M. Gajek, Q. He, L. W. Martin, S. Salahuddin, M. Trassin, S. Wu, and P. Yu. Additionally, we would like to express our gratitude to M. Viret and J. Wang for the permissions to reuse their works.

[1]K. Bernstein, R. K. Calvin III, W. Porod, A. Seabaugh, and J. Welser, Proc. IEEE **98**, 2169 (2010).
[2]S. A. Wolf, D. D. Awschalom, R. A. Buhrman, J. M. Daughton, S. von Molnar, M. L. Roukes, A. Y. Chtchelkanova, and D. M. Treger, Science **294**, 1488 (2001).
[3]D. D. Awschalom and M. E. Flatté, Nat. Phys. **3**, 153 (2007).
[4]A. Imre, G. Csaba, L. Ji, A. Orlov, G. H. Bernstein, and W. Porod, Science **311**, 205 (2006).
[5]D. Bhowmik, L. You, and S. Salahuddin, Nat. Nanotechnol. **9**, 59 (2014).
[6]B. Behin-Aein, D. Datta, S. Salahuddin, and S. Datta, Nat. Nanotechnol. **5**, 266 (2010).
[7]A. Khitun, D. E. Nikonov, and K. L. Wang, J. Appl. Phys. **106**, 123909 (2009).
[8]E. B. Myers, D. C. Ralph, J. A. Katine, R. N. Louie, and R. A. Buhrman, Science **285**, 867 (1999).
[9]Formed in 2002, Grandis (http://www.grandisinc.com) worked for several years to commercialize STT-RAM technology. In August 2011, Grandis was acquired by Samsung. D. McGrath, "Samsung buys MRAM developer Grandis" EETimes Aug, 2 2011 (http://www.eetimes.com/electronics-news/4218434/Samsung-buys-MRAM-developer-Grandis)
[10]S. S. P. Parkin, M. Hayashi, and L. Thomas, Science **320**, 190 (2008).
[11]D. C. Ralph and M. D. Stiles, J. Magn. Magn. Mater. **320**, 1190 (2008).
[12]J. C. Slonczewski, J. Magn. Magn. Mater. **159**, L1 (1996).
[13]H. Liu, D. Bedau, D. Backes, J. A. Katine, J. Langer, and A. D. Kent, Appl. Phys. Lett. **97**, 242510 (2010).
[14]G. E. Rowlands, T. Rahman, J. A. Katine, J. Langer, A. Lyle, H. Zhao, J. G. Alzate, A. A. Kovalev, Y. Tserkovnyak, Z. M. Zeng, H. W. Jiang, K. Galatsis, Y. M. Huai, P. Khalili Amiri, K. L. Wang, I. N. Krivorotov, and J.-P. Wang, Appl. Phys. Lett. **98**, 102509 (2011).
[15]K. F. Wang, J. M. Liu, and Z. F. Ren, Adv. Phys. **58**, 321 (2009).
[16]R. Ramesh and N. A. Spaldin, Nature Mater. **6**, 21 (2007).
[17]S.-W. Cheong and M. Mostovoy, Nature Mater. **6**, 13 (2007).
[18]H. Schmid, J. Phys.: Condens. Matter **20**, 434201 (2008).
[19]H. Béa, M. Gajek, M. Bibes, and A. Barthélémy, J. Phys.: Condens. Matter **20**, 434221 (2008).
[20]C. Binek and B. Doudin, J. Phys.: Condens. Matter **17**, L39 (2005).
[21]M. Fiebig, J. Phys. D: Appl. Phys. **38**, R123 (2005).
[22]W. Eerenstein, N. D. Mathur, and J. F. Scott, Nature **442**, 759 (2006).
[23]A. P. Pyatakov and A. K. Zvezdin, Phys.-Usp. **55**, 557 (2012).
[24]D. Khomskii, Physics **2**, 20 (2009).
[25]J. Ma, J. Hu, Z. Li, and C. W. Nan, Adv. Mater. **23**, 1062 (2011).
[26]N. X. Sun and G. Srinivasan, SPIN **2**, 1240004 (2012).
[27]C. A. F. Vaz, J. Phys.: Condens. Matter **24**, 333201 (2012).
[28]P. Royen and K. Swars, Angew. Chem. **69**, 779 (1957).
[29]J. Wang, J. B. Neaton, H. Zheng, V. Nagarajan, S. B. Ogale, B. Liu, D. Viehland, V. Vaithyanathan, D. G. Schlom, U. V. Waghmare, N. A. Spaldin, K. M. Rabe, M. Wuttig, and R. Ramesh, Science **299**, 1719 (2003).
[30]Y. F. Popov, A. K. Zvezdin, G. P. Vorobev, A. M. Kadomtseva, V. A. Murashev, and D. N. Rakov, JETP Lett. **57**, 69 (1993).
[31]C. Michel, J.-M. Moreau, G. D. Achenbach, R. Gerson, and W. J. James, Solid State Commun. **7**, 701 (1969).
[32]F. Kubel and H. Schmid, Acta Crystallogr., Sect. B: Struct. Sci. **46**, 698 (1990).
[33]J. R. Teague, R. Gerson, and W. J. James, Solid State Commun. **8**, 1073 (1970).
[34]I. Sosnowska, T. Peterlin-Neumaier, and E. Steichele, J. Phys. C: Solid State Phys. **15**, 4835 (1982).
[35]G. A. Smolenskii, V. M. Yudin, E. S. Sher, and Y. E. Stolypin, Sov. Phys. JETP **16**, 622 (1963).
[36]C. Ederer and N. A. Spaldin, Phys. Rev. B **71**, 060401(R) (2005).
[37]R. Seshadri and N. A. Hill, Chem. Mater. **13**, 2892 (2001).
[38]D. Khomskii, J. Magn. Magn. Mater. **306**, 1 (2006).
[39]P. Fischer, M. Polomska, I. Sosnowska, and M. Szymanski, J. Phys. C: Solid State Phys. **13**, 1931 (1980).
[40]I. E. Dzyaloshinskii, J. Phys. Chem. Solids **4**, 241 (1958).
[41]I. E. Dzyaloshinskii, Sov. Phys. JETP **19**, 960 (1964).
[42]T. Moriya, Phys. Rev. **120**, 91 (1960).
[43]C. Ederer and C. J. Fennie, J. Phys.: Condens. Matter **20**, 434219 (2008).
[44]C. J. Fennie, Phys. Rev. Lett. **100**, 167203 (2008).
[45]S. K. Streiffer, C. B. Parker, A. E. Romanov, M. J. Lefevre, L. Zhao, J. S. Speck, W. Pompe, C. M. Foster, and G. R. Bai, J. Appl. Phys. **83**, 2742 (1998).
[46]N. Balke, I. Bdikin, S. V. Kalinin, and A. L. Kholkin, J. Am. Ceram. Soc. **92**, 1629 (2009).
[47]L. W. Martin, Y. H. Chu, and R. Ramesh, Mater. Sci. Eng., R **68**, 89 (2010).
[48]L. W. Martin, Y. H. Chu, M. B. Holcomb, M. Huijben, P. Yu, S.-J. Han, D. Lee, S. X. Wang, and R. Ramesh, Nano Lett. **8**, 2050 (2008).
[49]W. H. Meiklejohn and C. P. Bean, Phys. Rev. **102**, 1413 (1956).
[50]J. C. S. Kools, IEEE Trans. Magn. **32**, 3165 (1996).
[51]S. S. P. Parkin, K. P. Roche, M. G. Samant, P. M. Rice, R. B. Beyers, R. E. Scheuerlein, E. J. O'Sullivan, S. L. Brown, J. Bucchigano, D. W. Abraham, Y. Lu, M. Rooks, P. L. Trouilloud, R. A. Wanner, and W. J. Gallagher, J. Appl. Phys. **85**, 5828 (1999).
[52]J. Nogues and I. K. Schuller, J. Magn. Magn. Mater. **192**, 203 (1999).
[53]A. E. Berkowitz and K. Takano, J. Magn. Magn. Mater. **200**, 552 (1999).
[54]M. Kiwi, J. Magn. Magn. Mater. **234**, 584 (2001).
[55]J. Stöhr and H. C. Siegmann, *Magnetism: From Fundamentals to Nanoscale Dynamics* (Springer, New York, 2006).
[56]C. Binek, *Ising-Type Antiferromagnets*, Springer Tracts in Modern Physics Vol. 196 (Springer-Verlag, Berlin, 2003), p. 55.
[57]J. Nogués, J. Sort, V. Langlais, V. Skumryev, S. Suriñach, J. S. Muñoz, and M. D. Baró, Phys. Rep. **422**, 65 (2005).
[58]E. C. Stoner and E. P. Wohlfarth, Nature **160**, 650 (1947).
[59]E. C. Stoner and E. P. Wohlfarth, Philos. Trans. R. Soc., A **240**, 599 (1948).
[60]A. P. Malozemoff, Phys. Rev. B **35**, 3679 (1987).
[61]A. P. Malozemoff, J. Appl. Phys. **63**, 3874 (1988).
[62]A. P. Malozemoff, Phys. Rev. B **37**, 7673 (1988).
[63]D. Schumacher, A. Steffen, J. Voigt, J. Schubert, and Th. Bruckel, Phys. Rev. B **88**, 144427 (2013).
[64]D. Mauri, H. C. Siegmann, P. S. Bagus, and E. Kay, J. Appl. Phys. **62**, 3047 (1987).
[65]F. Radu and H. Zabel, *Magnetic Heterostructures*, Springer Tracts in Modern Physics Vol. 227, edited by H. Zabel and S. D. Bader (Springer-Verlag, Berlin, 2007), p. 97.
[66]M. Daraktchiev, G. Catalan, and J. F. Scott, Ferroelectrics **375**, 122 (2008).
[67]G. Catalan and J. F. Scott, Adv. Mater. **21**, 2463 (2009).
[68]D. Lebeugle, A. Mougin, M. Viret, D. Colson, J. Allibe, H. Béa, E. Jacquet, C. Deranlot, M. Bibes, and A. Barthélémy, Phys. Rev. B **81**, 134411 (2010).
[69]D. Lebeugle, A. Mougin, M. Viret, D. Colson, and L. Ranno, Phys. Rev. Lett. **103**, 257601 (2009).
[70]H. Béa, M. Bibes, F. Ott, B. Dupé, X.-H. Zhu, S. Petit, S. Fusil, C. Deranlot, K. Bouzehouane, and A. Barthélémy, Phys. Rev. Lett. **100**, 017204 (2008).
[71]J. T. Heron, M. Trassin, K. Ashraf, M. Gajek, Q. He, S. Y. Yang, D. E. Nikonov, Y.-H. Chu, S. Salahuddin, and R. Ramesh, Phys. Rev. Lett. **107**, 217202 (2011).
[72]M. Trassin, J. D. Clarkson, S. R. Bowden, J. Liu, J. T. Heron, R. J. Paull, E. Arenholz, D. T. Pierce, and J. Unguris, Phys. Rev. B **87**, 134426 (2012).
[73]P. Yu, J.-S. Lee, S. Okamoto, M. D. Rossell, M. Huijben, C.-H. Yang, Q. He, J. X. Zhang, S. Y. Yang, M. J. Lee, Q. M. Ramasse, R. Erni, Y.-H. Chu, D. A. Arena, C.-C. Kao, L. W. Martin, and R. Ramesh, Phys. Rev. Lett. **105**, 027201 (2010).
[74]L. You, B. Wang, X. Zou, Z.-S. Lim, Y. Zhou, H. Ding, L. Chen, and J. Wang, Phys. Rev. B **88**, 184426 (2013).
[75]T. Zhao, A. Scholl, F. Zavaliche, K. Lee, M. Barry, A. Doran, M. P. Cruz, Y. H. Chu, C. Ederer, N. A. Spaldin, R. R. Das, D. M. Kim, S. H. Baek, C. B. Eom, and R. Ramesh, Nature Mater. **5**, 823 (2006).

[76]Q. He, C.-H. Yeh, J.-C. Yang, G. Singh-Bhalla, C.-W. Liang, P.-W. Chiu, G. Catalan, L. W. Martin, Y.-H. Chu, J. F. Scott, and R. Ramesh, Phys. Rev. Lett. **108**, 067203 (2012).
[77]Y.-H. Chu, Q. He, C.-H. Yang, P. Yu, L. W. Martin, P. Shafer, and R. Ramesh, Nano Lett. **9**, 1726 (2009).
[78]R. C. O'Handely, Solid State Commun. **21**, 1119 (1977).
[79]S. M. Wu, S. A. Cybart, P. Yu, M. D. Rossell, J. X. Zhang, R. Ramesh, and R. C. Dynes, Nature Mater. **9**, 756 (2010).
[80]J. Allibe, S. Fusil, K. Bouzehouane, C. Daumont, D. Sando, E. Jacquet, C. Deranlot, M. Bibes, and A. Barthélémy, Nano Lett. **12**, 1141 (2012).
[81]M. P. Cruz, Y.-H. Chu, J. X. Zhang, P. L. Yang, F. Zavaliche, Q. He, P. Shafer, L. Q. Chen, and R. Ramesh, Phys. Rev. Lett. **99**, 217601 (2007).
[82]T. L. Qu, Y. G. Zhao, P. Yu, H. C. Zhao, S. Zhang, and L. F. Yang, Appl. Phys. Lett. **100**, 242410 (2012).
[83]S. M. Wu, S. A. Cybart, D. Yi, J. M. Parker, R. Ramesh, and R. C. Dynes, Phys. Rev. Lett. **110**, 067202 (2013).
[84]M. J. Calderon, S. Liang, R. Yu, J. Salafranca, S. Dong, S. Yunoki, L. Brey, A. Moreo, and E. Dagotto, Phys. Rev. B **84**, 024422 (2011).
[85]G. Srinivasan, E. T. Rasmussen, B. J. Levin, and R. Hayes, Phys. Rev. B **65**, 134402 (2002).
[86]B. Dabrowski, L. Gladczuk, A. Wisniewski, Z. Bukowski, R. Dybzinski, A. Szewczyk, M. Gutowska, S. Kolesnik, C. W. Kimball, and H. Szymczak, J. Appl. Phys. **87**, 3011 (2000).
[87]W. Ratcliff II, Z. Yamani, V. Anbusathaiah, T. R. Gao, P. A. Kienzle, H. Cao, and I. Takeuchi, Phys. Rev. B **87**, 140405 (2013).
[88]D. Lebeugle, D. Colson, A. Forget, M. Viret, A. M. Bataille, and A. Gukasov, Phys. Rev. Lett. **100**, 227602 (2008).
[89]S. Lee, W. Ratcliff II, S.-W. Cheong, and V. Kiryukhin, Appl. Phys. Lett. **92**, 192906 (2008).
[90]V. Laukhin, V. Skumryev, X. Marti, D. Hrabovsky, F. Sanchez, M. V. Garcia-Cuenca, C. Ferrater, M. Varela, U. Luders, J. F. Bobo, and J. Fontcuberta, Phys. Rev. Lett. **97**, 227201 (2006).
[91]J. X. Zhang, Q. He, M. Trassin, W. Luo, D. Yi, M. D. Rossell, P. Yu, L. You, C. H. Wang, C. Y. Kuo, J. T. Heron, Z. Hu, R. J. Zeches, H. J. Lin, A. Tanaka, C. T. Chen, L. H. Tjeng, Y. H. Chu, and R. Ramesh, Phys. Rev. Lett. **107**, 147602 (2011).
[92]Y.-H. Chu, L. W. Martin, M. B. Holcomb, M. Gajek, S.-J. Han, Q. He, N. Balke, C.-H. Yang, D. Lee, W. Hu, Q. Zhan, P.-L. Yang, A. Fraile-Rodriguez, A. Scholl, S. X. Wang, and R. Ramesh, Nature Mater. **7**, 478 (2008).
[93]P. Shafer, F. Zavaliche, Y.-H. Chu, P.-L. Yang, M. P. Cruz, and R. Ramesh, Appl. Phys. Lett. **90**, 202909 (2007).
[94]L. You, E. Liang, R. Guo, D. Wu, K. Yao, L. Chen, and J. Wang, Appl. Phys. Lett. **97**, 062910 (2010).
[95]F. Johann, A. Morelli, and I. Vrejoiu, Phys. Status Solidi **249**, 2278 (2012).
[96]S. H. Baek, H. W. Jang, C. M. Folkman, Y. L. Li, B. Winchester, J. X. Zhang, Q. He, Y. H. Chu, C. T. Nelson, M. S. Rzchowski, X. Q. Pan, R. Ramesh, L. Q. Chen, and C. B. Eom, Nature Mater. **9**, 309 (2010).
[97]N. Balke, S. Choudhury, S. Jesse, M. Huijben, Y. H. Chu, A. P. Baddorf, L. Q. Chen, R. Ramesh, and S. V. Kalinin, Nat. Nanotechnol. **4**, 868 (2009).
[98]K. Ashraf and S. Salahuddin, J. Appl. Phys. **112**, 074102 (2012).
[99]T. R. McGuire and R. I. Potter, IEEE Trans. Magn. **11**, 1018 (1975).
[100]B. H. Miller and E. Dan Dahlberg, Appl. Phys. Lett. **69**, 3932 (1996).
[101]Y. H. Chu, Q. Zhan, C.-H. Yang, M. P. Cruz, L. W. Martin, T. Zhao, P. Yu, R. Ramesh, P. T. Joseph, I. N. Lin, W. Tian, and D. G. Schlom, Appl. Phys. Lett. **92**, 102909 (2008).
[102]Y. H. Chu, T. Zhao, M. P. Cruz, Q. Zhan, P. L. Yang, L. W. Martin, M. Huijben, C. H. Yang, F. Zavaliche, H. Zheng, and R. Ramesh, Appl. Phys. Lett. **90**, 252906 (2007).
[103]H. Li, X. Hu, Y. Wei, Z. Yu, X. Zhang, R. Droopad, A. A. Demkov, J. Edwards, K. Moore, W. Ooms, J. Kulik, and P. Fejes, J. Appl. Phys. **93**, 4521 (2003).
[104]M. P. Warusawithana, C. Cen, C. R. Sleasman, J. C. Woicik, Y. Li, L. F. Kourkoutis, J. A. Klug, H. Li, P. Ryan, L.-P. Wang, M. Bedzyk, D. A. Muller, L.-Q. Chen, J. Levy, and D. G. Schlom, Science **324**, 367–370 (2009).
[105]S. Couet, M. Bisht, M. Trekels, M. Menghini, C. Petermann, M. J. Van Bael, J.-P. Locquet, R. Rüffer, A. Vantomme, and K. Temst, Adv. Funct. Mater. **24**, 71 (2014).
[106]R. Ramesh, W. K. Chan, B. Wilkens, H. Gilchrist, T. Sands, J. M. Tarascon, and V. G. Keramidas, Appl. Phys. Lett. **61**, 1537 (1992).